Nanoparticle complex fluids

by
Eldrid Svåsand

Thesis submitted for the degree of
Philosophiae Doctor

Department of Physics
University of Oslo

April 2008

Series of dissertations submitted to the
Faculty of Mathematics and Natural Sciences, University of Oslo
Nr. 737

ISSN 1501-7710

Cover: Inger Sandved Anfinsen.
Printed in Norway: AiT e-dit AS, Oslo, 2008.

Produced in co-operation with Unipub AS.
The thesis is produced by Unipub AS merely in connection with the
thesis defence. Kindly direct all inquiries regarding the thesis to the copyright
holder or the unit which grants the doctorate.

Unipub AS is owned by
The University Foundation for Student Life (SiO)

Acknowledgement

This work was supported by the Norwegian Research Council through the Nanomat program (project-158541/431). The work was carried out at the Institute for Energy Technology.

Beginning this thesis I passed into a completely new world of physics which has widened my horizon substantially and given me a liking for carbon....

I would like to thank my supervisors Geir Helgesen and Arne Skjeltorp for enthusiastic guidance throughout this phd. Thank you for always being available for questions and discussions! A big thanks also to all the technical staff for always being so friendly and helpful! I would also like to thank the rest of the people at the physics department at IFE for a scientific and socially rich working environment!

I want to thank my parents Dagfrid and Lars for giving me the joy of learning! Without you I would probably not be writing this thesis...

Most of all, thank you Andrés for always being so patient and loving, and Matilde for encouraging efficient working hours and giving me lots of laughs!

Eldrid Svåsand
Oslo, April 2008

Contents

List of papers

Paper 1: G. Helgesen, K.D. Knudsen, J.P. Pinheiro, A.T. Skjeltorp, E. Svåsand, H. Heiberg-Andersen, A. Elgsaeter, T. Garberg, S. Nalum Naess, S. Raaen, M. F. Tverdal, X. Yu and T. B. Melø. *"Carbon Cones - a Structure with Unique Properties",* in Nanotubes and Related Nanostructures, edited by Yoke Khin Yap, Mater. Res. Soc. Symp. Proc. Volume **1057E**, Warrendale, PA, 2007.

Paper 2: E. Svåsand, G. Helgesen and A. T. Skjeltorp. *"Chain formation in a complex fluid containing carbon cones and disks in silicon oil",* Colloids and Surfaces A, **308**, 6770 (2007).

Paper 3: E. Svåsand, K. de Lange Kristiansen, Ø. G. Martinsen, S. Grimnes, G. Helgesen and A.T. Skjeltorp. *"Behavior of carbon cone particle dispersions in electric and magnetic fields"*, to be submitted.

Paper 4: E. Svåsand, J. Akselvoll, A. T. Skjeltorp and G. Helgesen. *"Local viscosity measurements using oscillating magnetic holes",* J.Applied Physics, **101**, 054910 (2007).

Technical report (TR): E.Svåsand, *"Scanning probe microscopes - a technical report"*, IFE-I 2008/004, April 2008.

List of symbols

τ	shear stress
τ_y	yield stress
$\dot{\gamma}$	shear rate
η	viscosity
η_a	apparent viscosity
η_0	bulk viscosity
η_s	viscosity of dispersant
η_{pl}	plastic viscosity
η_E	viscosity under applied electric field
η_{eff}	effective viscosity
$[\eta]$	intrinsic viscosity
ζ	$= (\mu_0 \sigma H)/(k_B T)$
Ψ	surface potential
Φ	volume fraction
Φ_m	maximum packing fraction
ε_s	permittivity of solvent
ε_p	permittivity of particle
ε_0	permittivity of free space
ε_r	relative permittivity
ε_{arf}	permittivity above the relaxation frequency
ε_{brf}	permittivity below the relaxation frequency
θ	angle
a	particle radius
V	particle volume
s	particle-particle separation
ρ	density
A	area of electrode/Hamaker constant
δ	closest particle-particle separation
v	particle velocity in x-direction
Σ_s	conductivity of solvent
Σ_p	conductivity of particle
R	electrical resistance
l	electrode separation
ω	angular velocity
m	disclination number
y	$= x/h$
α	exponent for ER/MR fluids
σ	magnetic dipole moment
χ_p	magnetic susceptibility of particles
χ_f	magnetic susceptibility of fluid
$\bar{\chi}$	effective magnetic susceptibility
$\mathbf{H}$	magnetic field
μ_0	magnetic permeability of vacuum
μ_f	magnetic permeability of fluid
k_B	Boltzmanns constant
Δ	exponent for ER fluids
U_0	magnetic dipolar potential
M	magnetization
M_s	saturation magnetization
M_0	spontaneous magnetization
C	capacitance
B	electrical susceptance, magnetic flux
u	electric dipole moment
E	electric field
T	temperature
W	particle interaction potential
β_{perm}	permittivity mismatch factor
Γ	ratio of particle to fluid conductivity
$\mathbf{e}_r$	unit vector
$\mathbf{e}_\theta$	unit vector
wt%	weight percent
f	frequency
h	distance between glass plates

Abstract

The work presented in this thesis concerns the study of complex nanofluids. The interaction of particles in dispersions under the influence of electric and magnetic fields has been studied. The main focus has been the investigation of the behavior of carbon particle dispersions.

A novel type of carbon material, namely carbon cone (CC) material, has been characterized using atomic force microscope, scanning tunneling microscope and scanning electron microscope. The CC material is a mixed powder consisting of carbon particles with the shape of disks and cones and a small amount of amorphous carbon particles. The length or diameter of the particles vary between 0.5-5 μm with thickness varying between 10-50 nm. The results confirm the cone angles as predicted by theory. The various microscopy images show that the surfaces of the particles seem corrugated. It should be noted that it is the mixed particle powder which it is referred to when it is written "carbon cone particles" or "CC particles".

The dispersion of CC particles in silicon oil was studied under the influence of an electric field. The particles were found to align in an ac electric field and structure formation was observed at very low electric fields. The growth rate was found to vary exponentially with the electric field. The structure formations were permanent(under zero shear rate), not dissolving when the electric field was turned off. This was attributed to the strong Van der Waals forces associated with carbon particles.

Electrorheological measurements were carried out for dispersions with varying CC particle concentrations. All samples showed a Bingham fluid behavior with a finite yield stress. The yield stress was found to depend only weakly on the electric field. The results showed that the ER efficiency as measured by the relative increase in viscosity compared to the zero field viscosity, increases with decreasing concentration with a maximum factor of $\sim$10 for the dispersion with lowest particle concentration. This is relatively low compared to commercial ER fluids and was attributed to the high conductivity of the particles and to the low relaxation frequency as determined by impedance measurements. The structure formations could be used to produce one dimensional conductive paths in composites.

Carbon cones were also dispersed in ferrofluid to observe their behavior in a magnetic field. A small increase in the viscosity was obtained for CC in a ferrofluid and this was attributed to purely hydrodynamic forces. No evidence of CC particle alignment was found.

The interaction of non-magnetic spherical particles (magnetic holes) in a ferrofluid was studied and used to develop a microrheological method for measuring the local viscosity of the ferrofluid itself. By using two magnetic holes which oscillate in a rotating magnetic field,

the apparent viscosity of the ferrofluid was determined. The advantage of this method is the small sample volume needed.

Chapter 1

Introduction

This work focuses on the study of rheological behavior of complex fluids, including electrorheological (ER) fluids and magnetorheological (MR) fluids including ferrofluids (FF). The main part concerns the use of a novel form of carbon, namely carbon cone (CC) material, as the solid phase in ER fluids. The CC material consists mainly of conical and disk shaped carbon particles. The particles have been mixed with silicon oil and studied under an applied electric field. The main purpose was to investigate the possibility of creating ordered structures formed under influence of an electric field. The resulting micro structures could be used as conductive paths in composites.

The second part concerns the investigation of CC particle behavior and interaction in a ferrofluid under an applied magnetic field and the development of a microrheological method employing the particle interaction of two oscillating magnetic holes for measuring the local viscosity of a ferrofluid.

Four scientific papers and one technical report are included in this thesis.

P1 gives an overview over the experimental work done on the CC material. The candidate has contributed with AFM/SEM characterization of the particles and the experimental work concerning the behavior of CC dispersions under an electric field. The candidate took part in the revision of the article.

P2 describes the chain formation of CC particles in silicon oil under an applied electric field. The growth rate vs electric field is described and a mechanism proposed. The candidate contributed with the complete experimental work and data analysis and wrote the first and edited versions of the article.

P3 is an electrorheological study of the system described in **P2**, but with samples of higher particle concentrations. The candidate contributed with all the experimental work except the magnetorheological measurements. The candidate carried out the data analysis of the ER measurements and wrote the first version of the article and edited versions together with the co-authors.

P4 concerns the interaction of two magnetic holes in a ferrofluid and how this interaction may be used to measure the local viscosity of the ferrofluid itself. The candidate has contributed to the article by carrying out the experimental work and analysis and writing the first version of the article and the edited versions together with the co-authors.

Technical report (TR): Characterization of the carbon material used was an important part of the work. This lead to intensive study and use of AFM/STM technique. The report gives a summary of the techniques and the results and is intended for internal use at the Institute for Energy Technology. It is therefor written in a more "popular" style.

Chapter 2

Complex fluids

Fluids that exhibit mechanical properties in between that of regular liquids and solids are often referred to as complex fluids. They may seem to be rather solid, but eventually begin to flow. Examples of complex fluids include mayonnaise, cheese, chocolate, blood, shampoo and tooth paste. Some complex fluids change character upon modest deformations or when an external force is applied. Fluids that respond to external electric or magnetic fields are called electrorheological (ER) fluids and magnetorheological (MR) fluids respectively. Both these kinds of fluids contain particles which interact due to an electric or magnetic moment, causing the dipole moment to align with the applied field. Neighboring particles will interact causing chain formation. This structure formation results in an apparent increase in viscosity due to the increased shear stress necessary to break the structures to cause the fluid to flow. The possibility of tuning the viscosity by controlling an external field, makes these kinds of fluids interesting for many applications ranging from automotive clutches to prosthetic knee dampers [1]. Another kind of complex magnetic fluid is the ferrofluid (FF) which consists of nanosized permanent magnetic particles in a organic or water based liquid. In a magnetic field the magnetic moments of the particles align with the field causing a net magnetization of the fluid. Due to the small sizes of the particles thermal motion hinders structure buildup at low magnetic fields hence no change in viscosity is observed. At high fields the apparent viscosity may increase substantially.

Research on complex fluids focuses on many aspects including the development of new materials suitable for electro or magnetorheological applications, understanding the interaction mechanisms of particle-particle and particle-fluid under an applied field and on the stability of these fluids. All of these aspects are important when considering an application.

This work is an experimental study concerning various nanoparticle dispersions and their behavior in an external field. The properties of a unique carbon powder consisting of conical and disk shaped particles and their electrorheological and magnetorheological effects in dispersions are studied. Also the interactions of non-magnetic spherical particles in a ferrofluid is investigated and used as a microrheological method to measure the local viscosity of the ferrofluid.

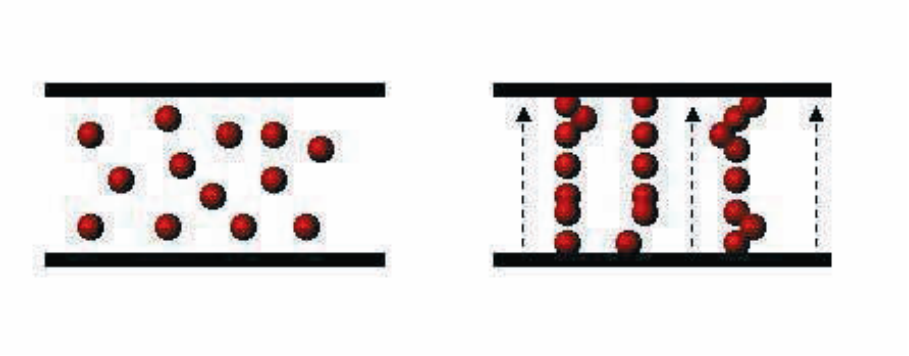

Figure 2.1: ER/MR fluid at zero field (left) and under an applied field (right).

2.1 Rheology

Rheology is the study of the deformation and flow of matter under the influence of an applied stress. Shear stress τ, is the force that a flowing liquid exerts on a surface, per unit area, in the direction parallel to the flow. The shear rate $\dot{\gamma}$, is the velocity gradient perpendicular to the direction of shear. For Newtonian fluids the relation between the shear stress and the shear rate is linear and is given by

$$\tau = \eta\dot{\gamma}, \tag{2.1}$$

where η is the viscosity. However most fluids do not show such behavior, meaning that η is a function of the shear rate, $\eta = \eta(\dot{\gamma})$, often called the shear viscosity. Such fluids are called Non-Newtonian fluids. Fluids where the viscosity decreases with increasing shear rate are called shear-thinning fluids. Fluids with the opposite behavior are called shear-thickening. Suspensions and emulsions are typically Non-Newtonian fluids.

Figure 2.2 shows the difference in shear response for Newtonian, shear-thinning, shear-thickening and Bingham fluids.

The viscosity of a fluid is also strongly temperature dependent. For Newtonian fluids the viscosity decreases for increasing temperature, approximately according to the relation

$$\eta = A\exp(\frac{-B}{T}), \tag{2.2}$$

where A and B are fluid dependent constants and T is the temperature. In general, the greater the viscosity, the stronger is the temperature dependence.

Bingham fluids are Non-Newtonian fluids characterized by a yield stress, τ_y. As opposed to Newtonian fluids they can transmit a shear stress without a velocity gradient. A Bingham fluid begins to flow only when the shear stress is larger than the yield stress. Hence the fluid behaves as a solid below the yield stress and as a liquid above. The relation between shear

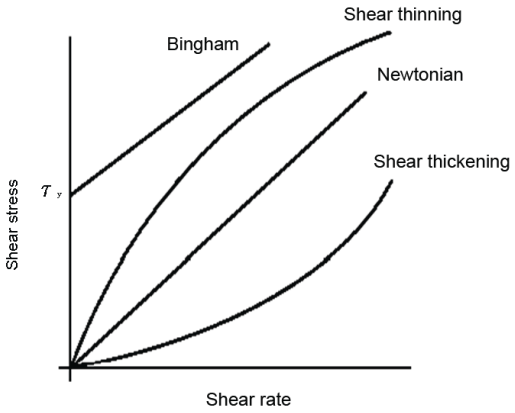

Figure 2.2: General flow chart of various kinds of fluid behaviors. The dynamic yield stress τ_y is characteristic for Bingham fluids and is found at the intersect with the y-axis.

stress and shear rate for a Bingham fluid is given by

$$\tau = \tau_y + \eta_{pl}\dot{\gamma}, \tag{2.3}$$

where η_{pl} is the plastic viscosity. It should be noted that in equation 2.3 the yield stress τ_y is the dynamic yield stress which is an extrapolated value from the plateau region in a plot (in log-scale) of shear stress vs. shear rate. The static yield stress is defined as the minimum shear stress required to induce continuous shear flow in an initially static sample. The two values are usually not equal [2].

2.1.1 Suspensions

For suspensions composed of ideal hard spheres the shear viscosity η may be predicted using the formula

$$\eta = \eta_s(1 + 2.5\Phi), \tag{2.4}$$

where η_s is the viscosity of the solvent and Φ is the particle volume fraction. This formulae is valid only for low volume fractions ($\Phi \leq 0.03$) as it assumes no particle-particle interaction. In the case of two neighboring spheres they will experience hydrodynamic interactions which leads to a contribution to η proportional to Φ^2. A more general empirical equation for the viscosity of suspensions of particles of any shape is the Krieger-Dougherty equation given by [3]

$$\eta = \eta_s(1 - \frac{\Phi}{\Phi_m})^{-[\eta]\Phi_m}, \tag{2.5}$$

where $[\eta]$ is the intrinsic viscosity defined by

$$[\eta] = \lim_{\Phi \to 0} \frac{\eta - \eta_s}{\Phi \eta_s}, \tag{2.6}$$

which depend on particle shape. For spheres $[\eta] = 2.5$. In equation (2.5) Φ_m is the maximum-packing volume fraction, which for hard spheres is $\Phi_m \approx 0.63 - 0.64$ [4]. As a general observation $[\eta]$ increases with particles aspect ratio, and Φ_m decreases. Hence the product $[\eta]\Phi_m$ usually remains in the range $1.4 - 3$.

2.2 Electrorheological fluids

2.2.1 Introduction

Winslow discovered the electrorheological (ER) effect in 1939 by chance. He observed that particles suspended in oils formed chain like structures when exposed to an electric field, and that the chains dissolved when the electric field was turned off again. His findings were patented in 1947 [5] and he published his observations in 1949 [6]. Due to his thorough description of the ER effect it is often named the Winslow effect.

ER fluids consist of an insulating fluid with a dispersed phase which may be liquid or solid. Solid phases used include silicate ceramics, conductive organics and polymers. Also carbonaceous particles as the dispersed phase have been studied, including cokes, carbon blacks, and fullerene type materials [7, 8, 9, 2, 10, 11]. The particles usually have sizes ranging from 0.1 to 100 μm. Volume fractions between 0.05 and 0.5 are common. When an electric field of 50-5000 V/mm is applied the particles interact with each other due to induced dipole moments. Depending on the angle between the direction of the field and the line connecting two neighboring particles the force will either be attractive or repulsive. The attractive forces cause the particles to form chain-like structures. The increased order of the suspension leads to an increase in the apparent viscosity which may be as high as 100000 times the viscosity at zero field, and the change may take place on the order of milliseconds. The rapid change from liquid to solid behavior makes ER fluids suitable for various applications. Certain properties are desirable for application purposes [12]; a) the ER fluid must show a high yield strength at a high electric field, b) low current density, c) strong ER effect in a wide temperature range, d) short response time and e) high stability. Current applications of ER fluids include clutches, brakes, damping devices, hydraulic vales and shock absorbers. In the following sections the ER mechanism, parameters influencing the ER effect and the characterization of ER fluids will be discussed.

2.2.2 Electrorheological Mechanisms

The physical mechanisms responsible for the ER effect are complex and still under dispute. There have traditionally been two main models that try to explain the ER mechanism, the polarization model and the conduction model. In addition there are other proposed mechanisms that may only partly explain the observed effects. These include explanation by electrophoresis due to net charge, overlap of electric double layers, and the water bridge mechanism.

The polarization mechanism [13, 14] explains the ER effect by a field induced polarization

of the particles relative to the fluid. The main parameter is the permittivity mismatch β_{perm} between the different phases given by

$$\beta_{perm} = \frac{\varepsilon_p - \varepsilon_s}{\varepsilon_p + 2\varepsilon_s}, \tag{2.7}$$

where ε_p and ε_s are the permittivities of the particles and solvent respectively. The polarization of the particles may be electronic, atomic, dipolar or due to interfacial charges, and the particle may be described as a dipole aligned with the electric field. Neighboring dipoles are attracted to each other when aligned with the field, resulting in a chain structure which leads to an increase in the apparent viscosity.

In the conduction model as proposed by Foulc and Atten [15] the important parameter is the conductivity mismatch Γ between the particles and the solvent given by;

$$\Gamma = \frac{\Sigma_p}{\Sigma_s}, \tag{2.8}$$

where Σ_p and Σ_s is the conductivity of the particle and the solvent respectively. A voltage drop occurs in the region between to neighboring particles producing a strong electric field. The conduction model lead to a linear variation of the force on the electric field at high fields ($>$ 1kV/mm). A parabolic dependency of the force is found at low fields ($<$ 1kV/mm).

The cause of the ER effect has also been explained by electrophoresis. Electrophoresis occurs when particles have a net surface charge. The charged particles will migrate to the electrode of opposite charge. This may result in a back and forth motion as many particles may change their charge upon contact with the electrode. The motion creates a secondary flow which increases energy dissipation leading to an increase in the apparent viscosity.

Klass and Martinek [16] explained the ER effect by the polarization of the double layer. A charged particle in a fluid will be surrounded by counter ions to balance its charge. This creates an electric double layer. This layer will be distorted under an electric field and interact with neighboring layers causing increased electrostatic repulsion which in turne increases the viscosity.

Water may create bridges between particles which may cause an increase in viscosity because of the work needed to overcome the surface tension of water in breaking the water bridges. This effect may partly explain some ER results, but cannot be the main mechanism as there also exist anhydrous ER fluids.

Recently a new model based on the effective dielectric constant formulation has successfully predicted yield stress, shear modulus and the real and imaginary parts of the dielectric constant of various systems [17]. The model relates the ER yield stress to the electrostatic energy of the system. This model may also describe the observed giant electrorheological effect (GER) as observed by Wen et al. [18] which is explained by surface saturation polarization. Hence more surface area would enhance the ER effect, which explains the strong effect seen with the nanosized particles.

In many cases the simple polarization model may explain many of the observed effects hence in the following section it is discussed in more detail.

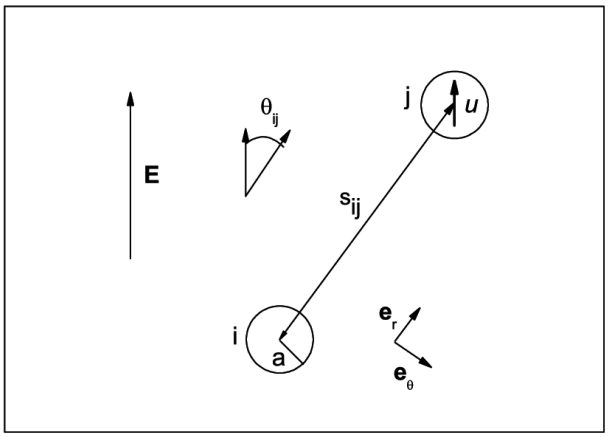

Figure 2.3: Explanation of symbols, vectors and unit vectors used in the polarization model.

Polarization model

Using the point-dipole approximation and assuming that $\varepsilon_p/\varepsilon_s$ is near unity the electric dipole moment u of an isolated sphere in a field E is given by

$$u = \beta a^3 E, \tag{2.9}$$

where β is given as in equation 2.7 and a is the particle radius. At dc fields or slow ac field β is determined by the conductivities rather than by the permittivities of the particles and medium [8].

The interaction potential between two particles i and j is given as

$$W_{i,j} = -\frac{4\pi\varepsilon_0\varepsilon_s u^2}{s_{ij}^3}(3\cos^2\theta_{ij} - 1), \tag{2.10}$$

where s_{ij} is the magnitude of the separation between the particle, ε_0 is the permittivity of space and θ_{ij} is the angle between the field and the line joining the two particles as shown in figure 2.3. The force on particle i produced by particle j is then given by

$$\mathbf{F_{ij}^{dipole}} = \frac{12\pi\varepsilon_0\varepsilon_s u^2}{s_{ij}^4}[(3\cos^2\theta_{ij} - 1)\mathbf{e_r} + \sin 2\theta_{ij}\mathbf{e}_\theta], \tag{2.11}$$

where $\mathbf{e_r}$ is a unit vector parallel to the line joining the centers of the two spheres and $\mathbf{e}_\theta$ is a unit vector perpendicular to $\mathbf{e_r}$.

The hydrodynamic forces may be approximated using Stokes' drag given by

$$\mathbf{F_i^{viscous}} = -6\pi\eta_s a\mathbf{v}, \tag{2.12}$$

Energy	Scale
Thermal	k_bT
London-van der Waals	$A/12\delta$
Electrostatic	$4\pi\varepsilon_0\varepsilon_s\Psi^2 a$
Polarization	$\pi\varepsilon_0\varepsilon_s a^3(\beta E)^2$
Viscous	$6\pi\eta_s a^3\mathbf{v}$

Table 2.1: Forces acting in an electrorheological suspension and their scaling.

where $\mathbf{v}$ is the velocity of the particle.

A steric repulsive force $\mathbf{F_i^{steric}} = \sum_{j\neq i} \mathbf{F_{ij}^{steric}}$ must also be included since the Stokes' drag approximation does not include lubrication forces produced when particles approach each other.

Brownian forces may be included when the particle sizes are below a certain value. In the present study the majority of the particles were too large for Brownian forces to be significant. By assuming the Hamakar constant to be $A = 5k_bT$ and δ=10 nm (δ=minimum particle-particle distance), we get the ratio between Brownian and van der Waals (vdw) forces to be Brownian/vdw$\approx 10^{-2}$. This shows that vdw forces are dominant over thermal forces in our system. Table 2.1 gives an overview over the characteristic inter-particle interaction energies in an ER suspension. Ψ is the surface potential.

2.2.3 Parameters influencing the electrorheological effect

Parameters which influence the ER effect are the dielectric properties and the conductivities of the fluid and particles, the viscosity of the fluid, the electric field (value and frequency), volume fraction of the particles, shape, size and surface charge of the particles. The influence of the dielectric properties on the ER effect has been studied by Ikazaki et al. [19] among others. They conclude that the ER effect increases with increasing $\Delta\varepsilon$ where

$$\Delta\varepsilon = \varepsilon_{brf} - \varepsilon_{arf}, \tag{2.13}$$

is the difference between the values of the dielectric constant at frequencies below (subscript *brf*) and above (subscript *arf*) the relaxation frequency of the ER fluid. The relaxation frequency of a good ER fluid is usually in the range $100 - 10^5$ Hz and is seen as a local maxima in the dielectric loss curve. Many studies concern the influence of particle shape on ER fluids [20, 9, 21]. Qi et al. [20] studied spheres and rods and found that in general the larger the particle that are used the stronger the ER effect. They also found that the shear stress for the spherical particles where much higher than that of the rod-based ER fluids. They explained this result as a result of entanglement of the rods, which led to less alignment. This is opposite to the findings by Wen et al. [18] where the giant electrorheological effect is observed using nanosized particles. Mustafa et al. [9] found that oblate graphite particles

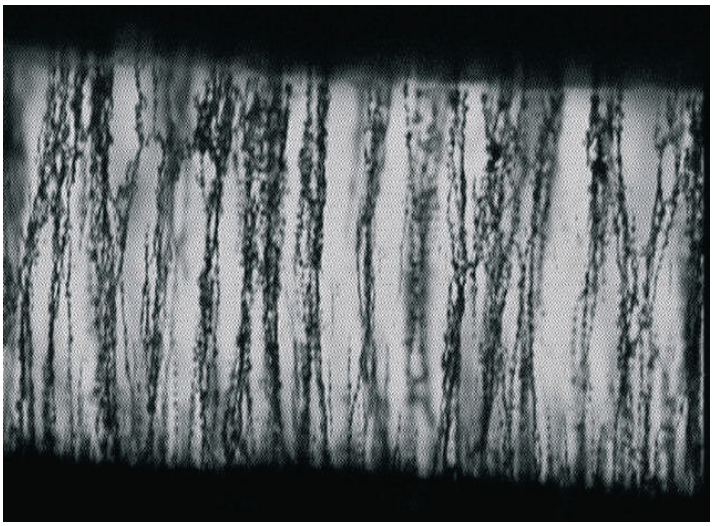

Figure 2.4: Carbon cone/disk chains formed at 58 V/mm, f=50 Hz.

in glycerol show higher apparent viscosity than in the case of nearly spherical particles. This was reversed when the particles were dispersed in water, proving that the viscosity of the dispersing fluid may influence the resulting ER effect. Lengalova et al. [21] studied particles of various materials with shapes of flakes, granules, globules and fragments all mixed with silicon oil. They found that at low shear rates, the viscosity of the flake particle ER fluids showed higher apparent viscosity than expected, which only could be explained from increased hydrodynamic interactions due to the asymmetry of the particles.

2.2.4 Characterization

There are several ways that the ER effect is studied and characterized. The most common is to carry out rheological measurements at zero field and at various electric fields, measuring the shear stress vs shear rate. The typical behavior of an electrorheological fluid under the influence of an external electric field is characterized by the Bingham fluid model. The constitutive equation for a Bingham fluid is

$$\tau(\dot{\gamma}, E_0) = \tau_y(E_0) + \eta_{pl}\dot{\gamma}, \tag{2.14}$$

for $\tau > \tau_y$, where E_0 is the applied electric field. The plastic viscosity η_{pl} will in general decrease with increasing shear rate, approaching the zero field viscosity for high shear rates. This shear-thinning behavior can be explained by chains or columns in the ER suspension which are gradually broken down by the increasing shearing.

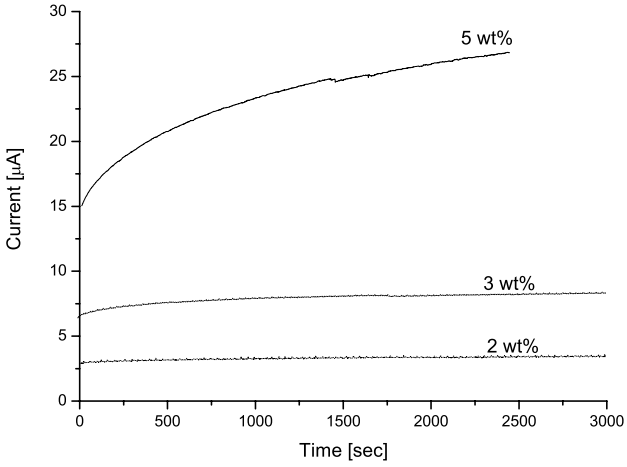

Figure 2.5: Increase in current with time for CC particles in silicon oil for samples with concentrations 2, 3 and 5 wt%. Electric field 58 V/mm and f=50 Hz .

The yield stress τ_y is found theoretically and experimentally to follow the relation

$$\tau(E_0) \propto \Phi^{\Delta} E_0^{\alpha}, \tag{2.15}$$

where Φ is the volume fraction of particles. The polarization model [13, 14] predicts that $\Delta = 1$ and $\alpha = 2$. For low and moderate field strengths $\alpha \approx 2$ has been observed. For high fields, the magnitude of α decreases somewhat [1]. The conduction model predicts $1 < \alpha < 2$ [15].

A typical value for the yield stress of commercial ER fluids is 1kPa at high field strengths. However in 2003 a new ER fluid with a yield stress of 130 kPa was made by researchers in China [18].

For application purposes the response time of the ER fluid is an important parameter. Some papers report on the visual observation of chain formation [18, 22] making it possible to study the chain growth rate. A dilute drop of the ER fluid is placed in a gap between two electrodes under a microscope and a video recording captures the process of chain formation.

The structure formation may also induce a conductive path through the insulating fluid. Hence a measure of the amount of ordered structure is given by the increase in conductivity vs time [23]. An example of increase in conductivity measured by the increase in current through the cell in samples of carbon cone particles in silicon oil, is shown in figure 2.5.

2.3 Magnetic fluids

In the literature the term magnetic fluids is many times used to describe both magnetorheological fluids(MR) and ferrofluids (FF). It must be noted that these two kinds of fluids are not equal and they show different behavior in a magnetic field. The next sections discusses the characteristics of MR fluids and ferrofluids and how they differ.

2.3.1 Magnetorheological fluids

MR fluids consist of 1-10 μm sized magnetically polarizable particles (typically carbonyl iron (CI)) in a carrier liquid. The liquid is usually a synthetic hydrocarbon liquid. Under an applied magnetic field the particles magnetize and align with the field. The particles interact with each other through dipole-dipole interactions leading to the formation of chains. The increased structural order causes an enormous change in the viscosity, on a timescale of milliseconds. When the field is removed, the original suspension and properties are restored. This mechanism was initially reported by Rabinow [24].

As for ER fluids, a magnetic polarization model may be used to describe the interaction causing the MR effect. Two magnetically polarized particles (i, j) with dipole moment σ have an interaction energy given by

$$W_{i,j} = -\frac{\sigma^2}{4\pi\mu_0 s_{ij}^3}(3\cos^2\theta_{ij} - 1), \tag{2.16}$$

where $\sigma = \frac{4}{3}\pi a^3 \mu_0 \chi_p H$, $\mu_0 = 4\pi \cdot 10^{-7}\mathrm{N/A^{-2}}$, χ_p is the magnetic susceptibility of the particles and H is the magnetic field.

Characterization of MR fluids is similar to that of ER fluids and it has been determined by Ginder et al. [25] that the yield stress scales with $H^{3/2}$ and not as H^2 due to the magnetic saturation. As discussed previously the yield stress of ER fluids scales with E^2 in most cases.

Applications using MR fluids include automotive clutch, brakes for exercise equipments, polishing fluids, seat dampers, prosthetic knee dampers, actuator systems and shock absorbers [1]. The main problem of MR applications is the cost of the carbonyl iron particles. Also in some applications the problem of particle sedimentation is crucial. This is not a problem for applications where the fluid is regularly shaken, but for applications like earthquake dampers where the fluid may be at rest for years. Recent production of new kind of MR fluid consisting of multiwalled nanotube [26] and single wall nanotube added carbonyl-iron suspension have been reported by Li et al. [27]. They found that the addition of SWNT reduced the sedimentation of CI without altering the MR properties. Another problem for application purposes is related to the oxidation of iron. If the particles are oxidized the magnetizability disappears.

2.3.2 Ferrofluids

The development of ferrofluids was a result of the necessity of NASA to have a moving liquid fuel in the gravity-free environment in space. In the 1960's NASA sponsored research

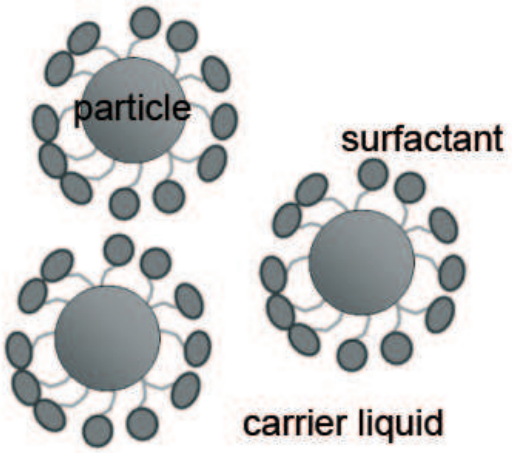

Figure 2.6: Nanosized particles with surfactant layer. Not drawn to scale.

which led to the development of ferrofluids. A ferrofluid consists of nanoscale ferromagnetic particles (typically magnetite particles) suspended in a liquid carrier, usually an organic solvent or water. A schematic figure of a ferrofluid is shown in figure 2.6. Other types of ferrofluids include metal in metal colloidal systems and paramagnetic salt solutions. In a conventional FF consisting of particles in a host liquid, the particles are coated with a suitable surfactant in order to prevent aggregation. The size of the particles are typically 10 nm, with the layer of surfactant being 2-3 nm thick. Each particle contains a single permanent ferromagnetic domain. The volume fraction of particles is typically around 7%, which, including the surfactant layer gives a hydrodynamic volume fraction of about 23% [28]. Ferrofluids differ from MR fluids in two ways; the magnetic field within each particle is permanent, and the particles are much smaller than particles used in MR fluids. Due to the small sizes of the particles Brownian motion disrupts the formation of chains keeping the viscosity unchanged at low fields, unlike MR fluids which become strongly viscous even under a low magnetic field. However, the nanoparticles experience strong forces in a magnetic field gradient and act as liquid magnets that are drawn into and held in place by a magnetic field.

Magnetic properties

The behavior of the ferrofluid depends mainly on the magnetic properties of the dispersed nanoparticles. In the absence of a magnetic field the particles rotate randomly due to Brownian forces. In a magnetic field H the magnetic moments σ of the particles will try to align with the field. This leads to a net magnetization M of the liquid. The magnetization of the liquid depends on the concentration of the magnetic particles, the temperature and

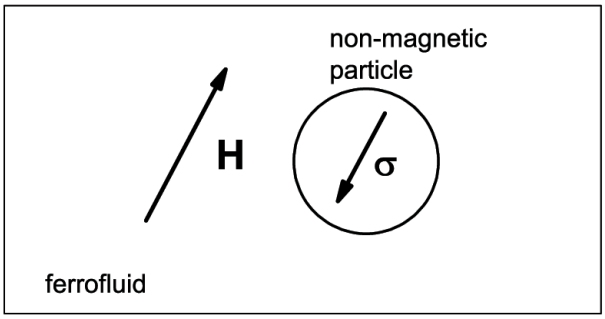

Figure 2.7: The magnetic moment of a magnetic hole or non-magnetic particle, pointing in opposite direction of the applied magnetic field.

on the saturation magnetization, M_s of the liquid. The magnetization of the fluid may be described by the Langevin law given by

$$M = M_s(\coth\zeta - \frac{1}{\alpha}), \tag{2.17}$$

where

$$\zeta = \frac{\mu_0 \sigma H}{k_B T}, \tag{2.18}$$

and $M_s = \Phi M_0$, Φ is the volume fraction of particles, M_0 is the spontaneous magnetization, T is the temperature and k_B is Boltzmann's constant [28].

The apparent viscosity of the ferrofluid is increased when the fluid is subjected to a shear flow under a strong magnetic field. If the flow is extensional, there is no viscosity increase. Since the force exerted by a magnetic field gradient on a magnetized system is proportional to its magnetization, ferrofluids experience strong magnetic forces even in weak magnetic fields due to their high initial susceptibility. In a homogeneous field no net force will act on the fluid, but if there is a magnetic field gradient the particles will be attracted to the region with the highest flux. This makes it possible to position and direct a ferrofluid with great accuracy. These properties have lead to applications of ferrofluids including seals and viscous dampers. In loud speakers ferrofluid is used to transfer heat from the coils. Material recycling also uses ferrofluids by taking advantage of the fact that the apparent density may change depending on the magnetic field strength. This is used to cause objects to sink or float, hence separation is achieved [29].

Magnetic holes in a ferrofluid

Magnetic holes have in this work been used in a microrheological method for determining the local viscosity of a ferrofluid. In the following a brief description of the theory used is given. For more details see **P4**.

When non-magnetic particles are immersed in a ferrofluid in an external magnetic field, they act as if they attain a magnetic moment σ of equal magnitude to but with opposite direction of that of the displaced volume of ferrofluid

$$\sigma = -V\bar{\chi}\boldsymbol{H}, \tag{2.19}$$

where $V = \pi a^3/6$ is the volume of a sphere of radius a and $\bar{\chi}$ is the effective magnetic susceptibility of the system. By using a rotating magnetic field magnetic holes will rotate or oscillate depending on the plane of rotation of the field. The interaction between two equal magnetic holes in an oscillating field may be described using the approximation of a dipole-dipole interaction given by

$$U_0 = \frac{\mu_f}{4\pi}\sigma^2\left(\frac{1-3\cos^2\theta}{s^3}\right), \tag{2.20}$$

where $\mu_f = \mu_0(1+\chi_f)$ is the magnetic permeability of the surrounding medium, s is the separation distance between the dipoles and θ is the angle between the separation vector and the direction of the field.

In the experiment described in **P4** the magnetic holes are in a confined geometry making it necessary to use the method of image dipoles in order to account for boundary effects. The magnetic holes and fluid are placed between two glass slides separated by a distance h. If we assume that the particle oscillate parallel to the direction of the horizontal field component we can set $s = x$. It is then convenient to introduce a dimensionless parameter $y = x/h$.

The strength of the potential given in equation (2.20) will oscillate with frequency 2ω between the two extremes, and can be rewritten as (for details see **P4**)

$$U(y,t) = \frac{1}{2}(U_{max}+U_{min}) + \frac{1}{2}(U_{max}-U_{min}), \cos(2\omega t). \tag{2.21}$$

where U_{min} and U_{min} are the minimum and maximum values of the magnetic potential. The resulting force on one particle may then be described by the amplitude of the oscillating magnetic force given by

$$F_{amp} = \frac{1}{4h}\left(\frac{dU_{min}}{dy} - \frac{dU_{max}}{dy}\right). \tag{2.22}$$

This magnetic force must be balanced by the hydrodynamic drag force given by

$$F_{visc} = -6\pi\eta_a a v, \tag{2.23}$$

were v is the velocity of the sphere in the x direction. Equation (2.23) is only true for isolated particles, hence in the present case a disturbance field produced by the second particle will influence the drag on the first particle. Hence, a correction factor is needed.

A sinecurve may be fitted to the experimental data which depicts the oscillation of the *separation distance* between the spheres. The fit is given by $y(t) = y_0 + y_{amp}sin(2\omega t)$, where

y_{amp} is the measured oscillation amplitude. The viscous force acting on each of the spheres, Eqn. (2.23), may then be rewritten as

$$F_{visc} = 3\pi a \eta_a h \frac{y_{amp}}{2} 2\omega, cos(2\omega t), \tag{2.24}$$

where v has been substituted by dy/dt. Equating the amplitudes of the magnetic and the viscous force, the apparent viscosity can be found as

$$\eta_a = \frac{\left(\frac{dU_{min}}{dy} - \frac{dU_{max}}{dy}\right)}{12\pi a h^2 \omega y_{amp}}. \tag{2.25}$$

The bulk liquid viscosity η_0 can thus be obtained from the apparent viscosity η_a by correcting for the disturbance field and confined geometry [30].

Chapter 3

Carbon materials

Carbon is an abundant nonmetallic, tetravalent element. It has different allotropic forms, the most known being diamond and graphite. Figure 3.1 shows some of the carbon allotropes. The very different properties of diamond and graphite is due to the atomic arrangement of the carbon atoms. In diamond the atoms have a tetragonal arrangement which gives the diamond its hardness. While in graphite the carbon atoms form an hexagonal network in separate layers which are loosely bound making it possible to write with a graphite pencil. The two allotropes buckyballs and nanotubes have been, and currently are, the focus of intensive research due to their very unique structures. The buckyballs were discovered in 1985 [32] and the nanotubes in 1991 [33]. In 1994 [34] a new allotrope of carbon with the form of a cones was discovered. All of these structures are composed of carbon atoms, only varying in the atomic arrangement of the atoms.

In the following the CC material which includes carbon cones and disks will be described in more detail together with carbon nanotubes.

3.1 Carbon cone material

Carbon with a conical form exist in many different forms [35, 34, 36, 37]. In this work carbon cone particles found in the CC material refers to hollow conical structures consisting of multiple layers of graphene sheets. This type of cones where discovered in 1994 [34] in small quantities, and i 1995 in industrial quantities in the so-called Kværner Carbon Black & Hydrogen Process [38]. The cones represent perfect conical structures and consist of curved graphene sheets formed as hollow cones with a closed tip.

Due to pure topological constraints there exist five discrete cone angles. If sectors of multiples of 60° are removed from a planar graphene sheet, and the free bonds are reconnected, conical structures are formed. The number of sections removed, m, is equal to the disclination number. The disclination creates a necessity of incorporating pentagons in the tip, in order for the structure to be closed. The number of pentagons incorporated correspond to the disclination number. Hence cones with 1-5 pentagons incorporated give cones with apex angles of $112.9°, 83.6°, 60°, 38°$, and $19.2°$, respectively. $m = 0$ gives planar disks, or

equivalently apex angle of 180°, and $m = 6$ gives half spheres found at the end of closed nanotubes. SEM images of the carbon cones with $m = 0 - 5$ is shown in figure 3.2. In figure 3.3 the distribution of the occurrence of the cone angles, as determined from SEM observations is shown. It should be noted that the distribution of the occurrence of specific cone angles varies between different production batches. Unfortunately the production parameters for the various batches are not known. The cones are typically 0.5- 1 μm long, but also cones with a length of 3 μm have been observed. The wall thickness is around 10-50 nm. The diameter of the disks are in general between 1 and 5 μm, but disks with a diameter of 10 μm has also been observed. The thickness is similar to that of the cones.

Element analysis done by energy dispersive spectroscopy (EDS) shows the possible presence of Al, Si and S atoms. The values of Al and Si are both within the uncertainty of the instrument but contamination of S is a fact. However the purity of the sample is above 99%. Because of their perfect shape, theory predicts that the cones are likely to have unique properties which could be useful in various applications like sensors, field emission probes, AFM/STM tips and as hydrogen storage material [39].

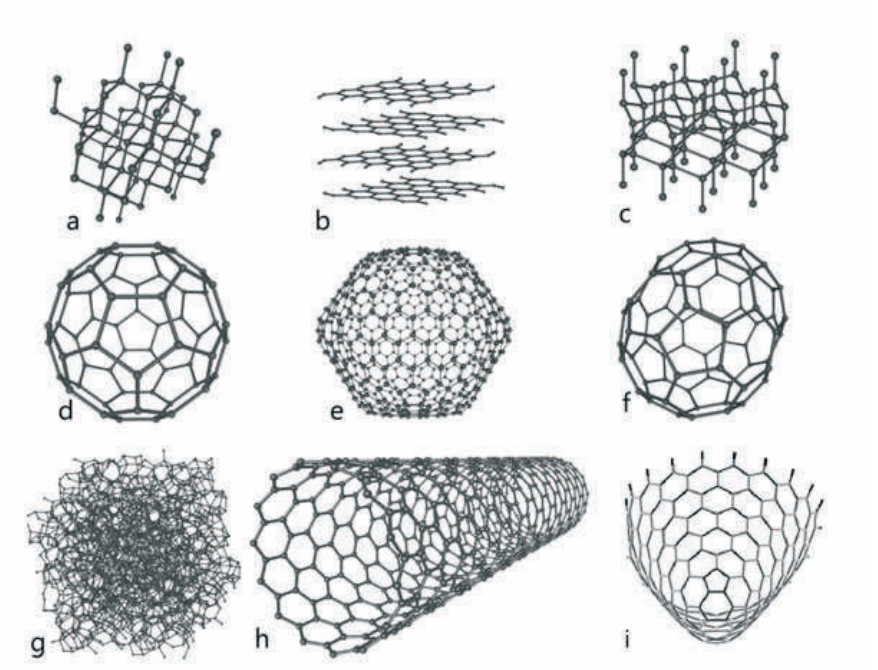

Figure 3.1: Some allotropes of carbon: a) diamond; b) graphite; c) lonsdaleite; d-f) fullerenes (C60, C540, C70); g) amorphous carbon; h) carbon nanotube i) cones. Adapted from [31].

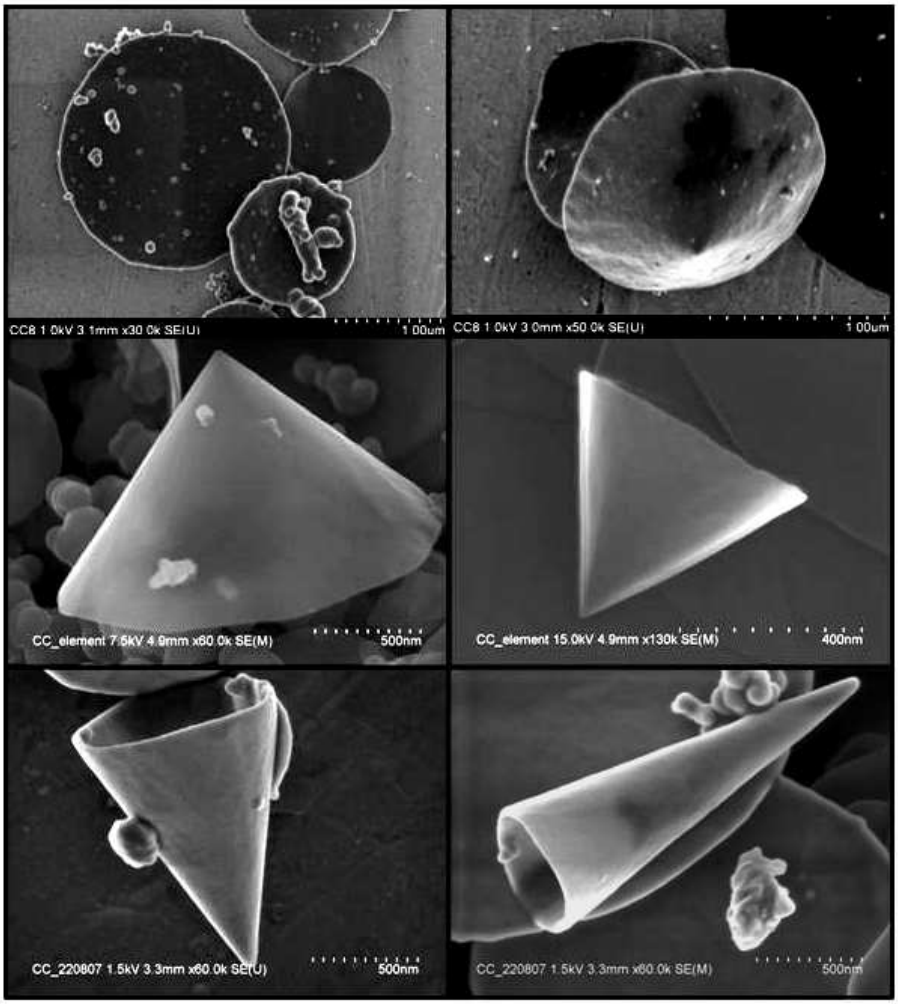

Figure 3.2: SEM images of carbon disk $m = 0$, and carbon cones with $m = 1 - 5$ pentagons, from left to right, top to bottom.

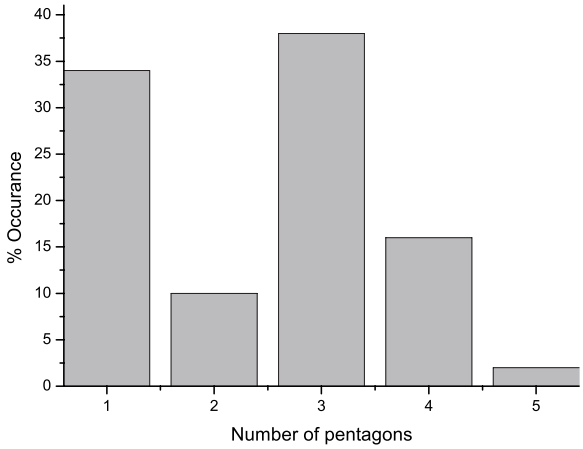

Figure 3.3: Distribution of the occurrence of the 5 types of cones.

Element	weight %	Atom %
C	99.16	99.68
Al	0.05	0.02
Si	0.10	0.04
S	0.68	0.26
Total	100.00	100.00

Table 3.1: Elemental analysis of the carbon cones particles.

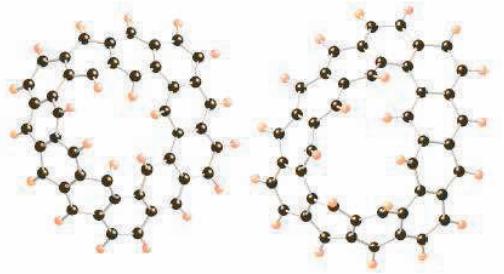

Figure 3.4: Example of two carbon rings with added carbon atoms on the edges. Both rings leads to a dislocation $m = 2$, before pentagons are incorporated. Adapted from [44].

Production of carbon cones

The cones used in this work were produced in the Kværner Carbon black & Hydrogen process [40]. This process consist in the pyrolysis of hydrocarbons in an carbon arc. The reactor pressure is at about 2-3 bar. The effective plasma temperature is estimated to be a least 2000°C. The products from the process are carbon cones, disks, amorphous carbon and minute amount of tubes [38]. The relative amounts of the different carbon shapes are 70 % disks, 20 % cones and 10% amorphous carbon and tubes [41].

The nucleation of the carbon cones is still a puzzle. There exist three models which try to explain how the curved graphite structures may form; the pentagon-road model, the ring-stacking model and a model based on Gibbs free energy. The pentagon-road model assumes that initially a planar graphite sheet is formed. Due to the energy of the dangling bonds at the edges of the sheet the structure will fold up and incorporate pentagons in order to eliminate the bonds. A problem with this model is the explanation of the initial formation of the planar sheets. In addition, total energy calculations by Fan et al. [42] suggest that pentagons are incorporated into the structures at a very early stage. Hence, it gets difficult to justify the initial planar sheet.

The ring-stacking model as proposed by Wakabayashi and Achiba [43] focuses on the selective assembly of monocyclic carbon rings. The formation is driven by entropy changes.

Treacy and Kilian [44] describe a model based on Gibbs free energy. They suggest the starting point of the cones to be carbon rings with n carbon atoms (C_n-rings)(figure 3.4). As additional carbon atoms are attached to the ring, the structure stiffens giving rice to a disclination. The pentagons are incorporated after the nucleation of this disclination. The large flexibility of the rings gives many pathways of forming a cone, which increases the entropy. This proves that the formation of cones with higher enthalpy of formation still may be favorable due to the resulting decrease in Gibbs free energy. The fact that the sample consist of mostly disks may be explained by having a low concentration of C-rings in an abundant supply of graphitic carbon building units (C and C_2). Graphite will form by self

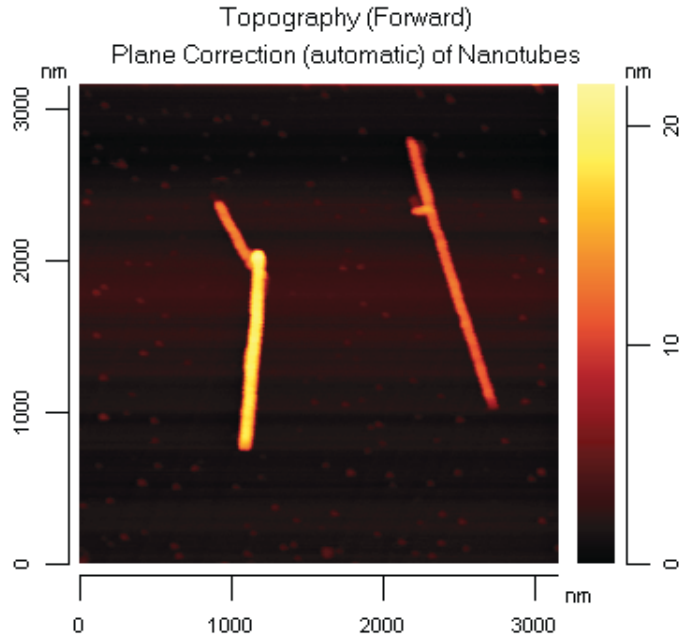

Figure 3.5: AFM topography image of multiwall nanotubes.

assembly of small carbon units. Addition of C and C_2 to the C_n-rings give rise to the conical structures when $n < 30$.

3.2 Carbon nanotubes

Carbon nanotubes (CNT) were discovered in 1991 by Iijima [33]. The tubes consist of a rolled up sheet of graphene. There are two main types of carbon nanotubes; single wall nanotubes (SWNT) and multiwall carbon nanotubes (MWNT). Their diameter may vary from only a few nanometer to about 50 nm for MWNT and their length is usually a couple of micrometers but may be grown to, what seems like, infinitely long [**?**].

The tubes are light, flexible, thermally stabile, and chemically inert. The SWNT's may be either metallic or semi-conducting depending on the "twist" (helicity) of the tube. Like graphite the nanotubes are also composed entirely of sp2-bonds. This bonding gives the nanotubes a unique strength. The pi orbital electrons delocalized across the hexagonal atomic sheets of carbon contribute the graphite's conductivity. Some properties of SWNTs MWNTs are given in table 3.2.

Property	SWNT	MWNT
Diameter	1.2-1.4 nm	10-50 nm
Tensile strength	30 GPa	63 GPa
Elastic modulus	1 TPa	1 TPa
Gap semiconducter	0.5 eV	
Resistivity	$10^{-4}\Omega$cm	
Thermal conductivity	2000 W/(m K)	

Table 3.2: Properties of SWNT and MWNT [45].

Due to the unique properties of the carbon nanotubes there has been intensive research going on since the discovery in 1991. Many promises of applications have been given but at present there are only a few applications on the marked, despite the large effort. This is mainly due to the difficulties in up-scaling the production of nanotubes.

Production of carbon nanotubes

Carbon nanotubes may be produced by electric arc discharge method, laser-assisted methods or by vapor deposition.

In the arc discharge method an electric arc produces a temperature of up to 4000°C and creates nanotubes through arc-vaporization of two carbon rods placed end to end, separated by approximately 1 mm. The voltage is typically 20-30 V. The electrodes are placed in an inert gas (helium/ argon) atmosphere. Carbon tubes and other nano-particles are formed [46]. The yield is up to 30 wt% and both single and multiwalled tubes with lengths up to 50 μm are produced [47].

In Laser-assisted synthesis a laser beam, pulsed or continuous, is targeted at a graphite rod that is contained in a tube. The tube is evacuated and at the same time heated to a temperature of 1200°C. Argon or Helium gas is supplied to the tube in order to keep a pressure of 500 torr. The laser vaporizes the graphite rod giving a product consisting of nanotubes and nanoparticles. The product is collected on a cooled copper finger, on the walls of the tube and on the reverse side of the graphite target [48]. When pure graphite rods are used only MWNT are formed. If the rods consists of a mixture of graphite and Co, Ni, Fe or Y, SWNT are formed. Nanotubes produced by laser ablation are purer than tubes produced by the arc-discharge technique. The SWNT also have better properties and a narrower size distribution then SWNT produced by arc-discharge method [46]. The yield is around 70 wt% and it is mainly SWNTs that are produced by this method. However this method is more expensive than both arc discharge or CVD deposition [47].

Chemical vapor deposition (CVD) is a method where a plasma or heated coil is used to transfer energy to a carbon molecule in gaseous form (methane, carbon monoxide etc). The energy causes the molecule to "crack" into reactive carbon atoms. The carbon then diffuses to a heated substrate coated with a catalyst. By properly adjusting various parameters such as the catalyst, SWNT rather than MWNT may be produced. Controlling the diameter is

also possible.

Chapter 4

The Experiments

In this chapter the various experiments conducted during this thesis are presented. In section 4.1 an experiment concerning electrophoresis of CC is reviewed. This was rather unsuccessful, but lead to the experiments concerning electrorheology of CC which are presented in section 4.2. Hence I find it appropriate to mention it. A short description of the experiment concerning viscosity measurement of ferrofluids is given in section 4.3, and a more detailed description is given in **P4**. Section 4.3.1 gives a short review of CC added ferrofluid and its magnetorheology. Lastly, in section 4.4 characterization of single particles are described. This was actually the first part of the work of this thesis, but since it was not the main focus of the work but rather a continuous process, it is presented last. AFM/STM characterization is not reviewed in section 4.4 as it is presented separately in the **technical rapport** included in the paper section.

4.1 Separation of carbon cones and disks by electrophoresis

Motivation

As the CC material is a mixture of disk shaped, conical shaped and amorphous carbon particles, we wanted to investigate the possibility of particle separation using electrophoresis. This method has been employed by others for separation of metallic and semiconducting SWNT [49]. Ideally, theory predicts carbon cones to have an electrostatic dipole moment associated with it [50]. One would therefore expect that the forces acting on the disks and cones in dispersion in an electric field to vary due to variable drag coefficients and due to unequal dipole moments of the particles.

Set-up

Figure 4.1 shows the commercially available finger-electrodes used (IAME 2004.3 series, Abtech scientific). The electrodes (Au) were 3 mm long, 20 μm wide and the electrode

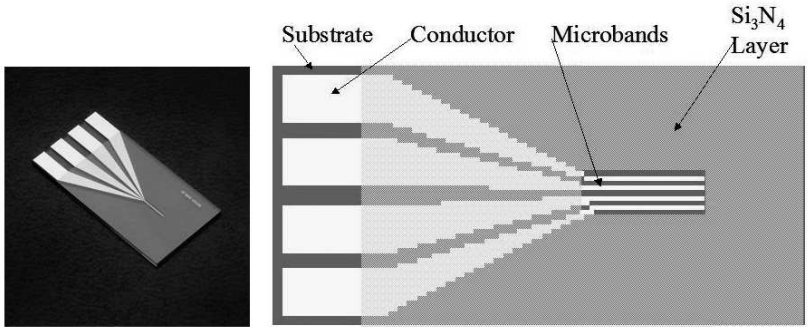

Figure 4.1: Photo and schematic drawing of the IAME chip. The chip size is (l,w,t) 1.00 x 2.00 x 0.05 cm and the microbands are 20 μm wide and 3 mm long.

separation was 20 μm. By employing an adhesive and using a thin glass plate, a closed cell was made. A dilute sample of mixed CC particles in isopropanol was put in the cell, the cell was closed and a dc power supply connected. Electric fields between $5 \cdot 10^4 - 2 \cdot 10^5$ V/mm were used. The sample cell was placed on a microscope with a digital camera set-up, as shown in figure 4.4. The particles were tracked using a matlab program. Only particles with a chosen minimum displacement between two consecutive frames were tracked. An image of the cell showing particle tracks is seen in figure 4.2.

Results and discussion

When an electric field was applied the particles moved to the positive electrode, indicating that they have a negative charge. This has also been reported by Lau et al. [51] who claims the negative charge formed on carbon in isopropanol is due to hydroxyl groups forming on edges. Due to the large particle size, some particle sedimented before reaching the electrode. The experiments proved to be difficult due to many factors. First, as the size of the particles are in the limit of the resolution of the microscope it was impossible to observe which particle types, cones or disks, that were moving. Hence, a second attempt was made opening the cell after the electrophoresis so that the particles could be observed using the SEM. This was also problematic due to the disturbance of the fluid created when opening the cell, which could remove/move particles from the electrodes. Also, since the chip substrate was not conductive, charging of the particles in the SEM made imaging difficult. A second factor was the dilute samples. The samples had to be dilute in order to be able to observe single particles. But as the concentration of cones were low it was difficult to get enough data to make any reliable statistics on differences in particle mobilities.

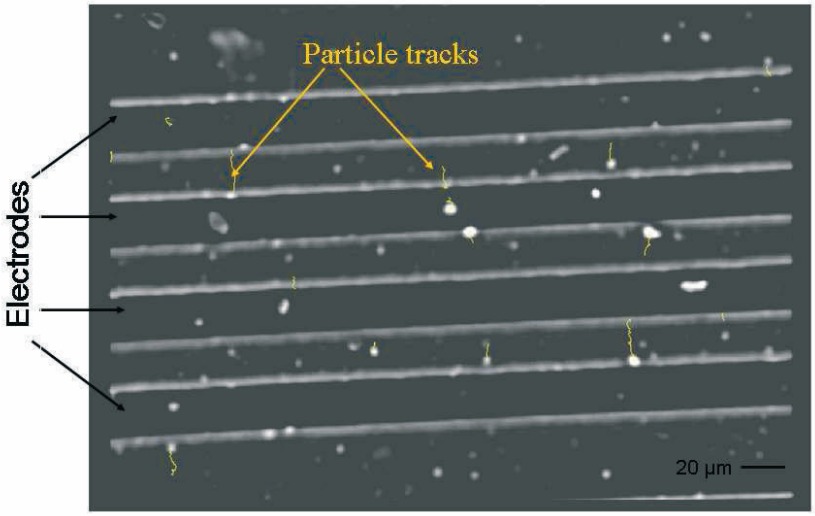

Figure 4.2: Particle tracking during electrophoresis of CC in silicon oil. The yellow lines represent particle movement.

Lessons learned

The electrophoresis experiment gave us some basic insights into the system that we could take advantage of during the next experiments, like the determination of a net negative charge on the particles and the ease of dispersing CC particles in isopropanol. It is also clear now that in order to have any chance of particle separation using electrophoresis the setup would also have to be different, with a much longer flow pathway for the particles. Also an improved method for particle detection with i.e tagging of the conical particles is necessary in order to distinguish between the different particle types.

4.2 Behavior of carbon cone dispersions in an electric field

The following section gives a brief introduction to the experimental work published in papers **P2** and **P3**. The investigation of the electrorheological (ER) effect of carbon cones in silicon oil was the topic of paper **P2** and **P3**. This was motivated by the possibility of inducing ordered structures i.e. one dimensional conductive paths in composites. Carrying out electrorheological measurements makes it possible to determine the kinetics and the interaction strength (rigidity) of the structures formed under an electric field. In the following a brief description of the experimental setup and an overview of the results is given. More

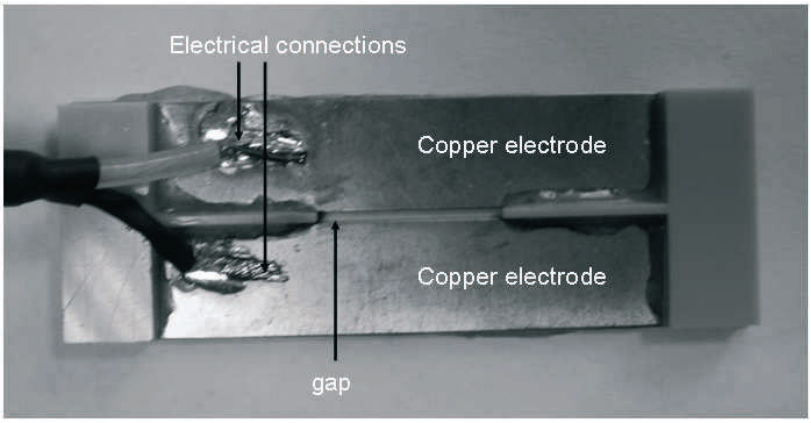

Figure 4.3: The cell used for chain formation observations. The width of the electrodes is 1,3 cm and the length is 5,5 cm. The gap on this cell was 1 mm.

details are found in the respective articles.

4.2.1 Chain formation

A qualitative experiment concerning the investigation of chain formation was carried out as described in **P2**. This should prove whether the CC particles are polarized in an electric field or not. A cell consisting of copper electrodes glued onto a microscope slide was used (figure 4.4) The electrodes were 1.3 cm wide, 5.5 cm long and 0.3 mm thick. By varying the gap between the electrodes and by varying the applied ac voltage, an electric field of 50-1000 V/mm could be applied. The frequencies used where 1, 10, 50, 500 and 1000 Hz. An ac-field was used due to observed electrophoresis at dc fields during pre-experiments as mentioned in the previous section. After mixing of the carbon cone particles with silicon oil using ultrasound (20 min., 30 W), a drop of the dispersion was placed in the gap of the cell and the system allowed to stabilize. Then digital video recording was carried out while an electric field was applied. The chain lengths were measured from the video images and plotted as a function of time after the onset of the electric field. A typical image series demonstrating the evolution of chain formation is presented in figure 4.5a.

Results and discussion

The result showed that the carbon cone particles do form chains in an ac electric field in the frequency range tested here (1-1000 Hz). An interesting result was that the formation of chains were observed even at fields as low as 50 V/mm (figure 4.5). For most reported ER

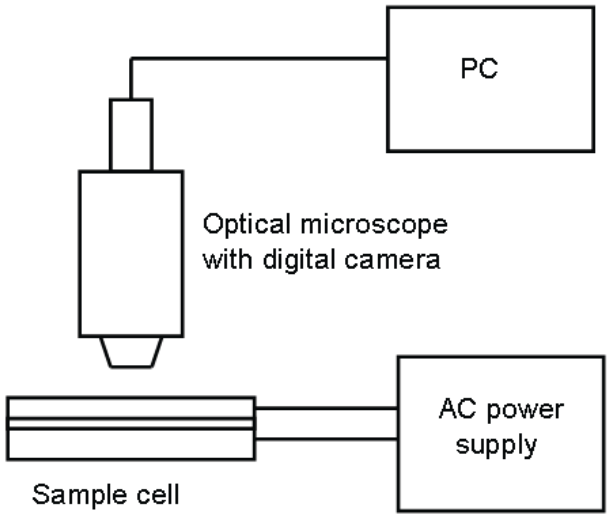

Figure 4.4: Schematic drawing of the experimental setup during study of chain formation of CC in silicon oil.

fluids a minimum electric field of about 0.5 kV/mm is need for chains to form. The chain growth rate increased exponentially with the electric field E as expected. No significant variation in growth rate was found when varying the frequency for values f <500 Hz. Above 500 Hz the growth rate decreased with increasing frequency (not shown). The experiments also showed that the dispersion does not return to its original state when the electric field is turned off. This was attributed to the strong attraction forces between carbon particles due to Van der Waals forces. Using ultrasonnication the dispersion again returned to its original state with well dispersed particles.

4.2.2 Electrorheology

P3 describes the investigation of the electrorheological effect of CC particles in silicone oil. To determine the induced viscosity change as a result of the chain formation, samples with CC particle concentration varying between 0.2 and 2.5 wt% were investigated using ER measurements. A rheometer (Physica MCR 300) equipped with an ER cell with concentric cylinder geometry was used, see figure 4.6. The gap between the cylinder and the cup was 1.13 mm. The viscosities of the samples were measured at 25°C. The setup was connected to an ac-power supply with a fixed frequency of 50 Hz. The ER cell was filled with the dispersion and a pre-shear experiment at zero field was carried out. Then the electric field was applied across the gap for 3 minutes to allow for chain formation. After 3 minutes the inner cylinder started to rotate, increasing the speed in a ramp logarithmic manner from

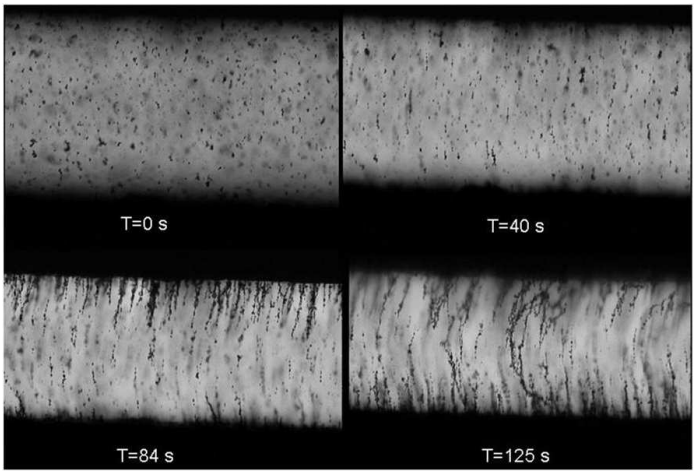

(a)

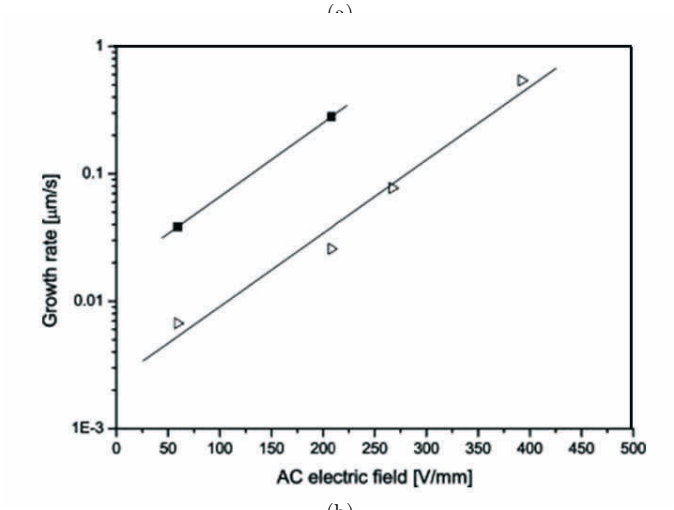

(b)

Figure 4.5: a) Chain evolution of 0.1 wt% CC in silicon oil at E=267 V/mm and 50 Hz. b) Growth rate of chains vs electric field for samples with CC concentrations 0.1 wt% (triangle) and 0.14 wt% (filled square).

Figure 4.6: The rheometer used for electro and magnetorheological measurements.

0.01 Hz to 1000 Hz. The shear stress vs shear rate curves were collected for the samples at electric field strengths of 100, 200 and 300 V/mm. Between each measurements the samples were sonnicated for 20 minutes to assure a good dispersion of the particles.

Results and discussion

The flow curve for a dispersion of 0.2 wt% CC in silicon oil is shown in figure 4.7. At zero field the sample behaved as a Newtonian fluid. When exposed to an electric field the dispersion showed a typical Bingham fluid behavior with a dynamic yield stress of roughly ∼1 Pa at 300 V/mm. The flow curves for the other sample concentrations showed similar behavior. The ER effect as measured by the yield stress, increases with increasing concentration as may be seen in figure 4.8. This is as expected. The yield stress scales as $\sim E^{\alpha}$ where α is between 0.36 and 0.68. The low value of α shows a weak dependence of the yield stress on the electric field. The relative ER effect as measured by the relative increase in yield stress is low compared to commercial ER fluids that may have an increase in the yield stress of a factor $\sim 10^3$. According to Lan et al. [52] there exists a critical ratio Γ_c where $\Gamma = \Sigma_p/\Sigma_s$, which gives the maximum shear stress. Here, Σ_p and Σ_s are the conductivities of the particles and dispersant respectively. For $\Gamma > \Gamma_c$ the ER effect decreases again. According to Lan the ER effect occurs when Γ varies in the $1 \cdot 10^3 - 4 \cdot 10^5$ range. In our system $\Sigma_p = 0.2$ S/m and $\Sigma_s \sim 10^{-12}$ giving $\Gamma \sim 10^{11}$. Despite the high Γ value we still observe ER effect, but the effect is weak and that is attributed to the high conductivity of the particles.

The ER efficiency is given by the effective viscosity

$$\eta_{eff} = (\eta_E - \eta_0)/\eta_0, \tag{4.1}$$

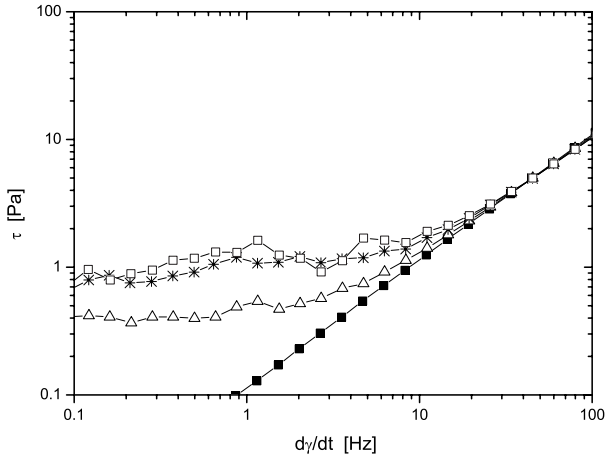

Figure 4.7: Shear stress vs shear rate for 0.2 wt% CC in silicon oil with η_s=100 mPa s, at various electric fields, all at 50 Hz. 0 V/mm (filled square), 100 V/mm (triangle), 200 V/mm (star) and 300 V/mm (empty square).

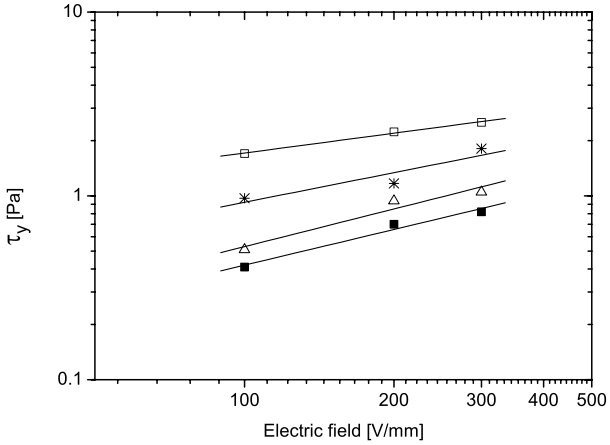

Figure 4.8: The yield stress vs electric field for samples with CC particle concentration of 0.2 wt% (filled square), 0.5 wt% (triangle), 1.1 wt% (star) and 2.5 wt% (empty square).

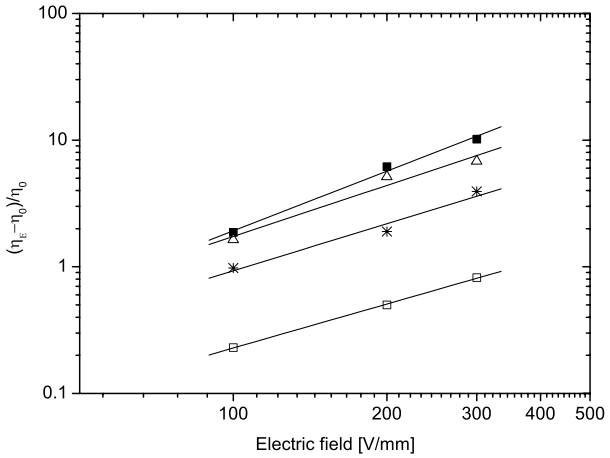

Figure 4.9: ER efficiency $(\eta_E - \eta_0)/\eta_0$, measured at $\dot{\gamma}$=1 Hz for samples of variable concentrations; 0.2 wt% (filled square), 0.5 wt% (triangle), 1.1 wt% (star) and 2.5 wt% (empty square).

where η_E is the viscosity measured at an electric field E and η_0 is the zero field viscosity. η_{eff} increases for decreasing concentrations as seen in figure 4.9 and was found to scale as $\eta_{eff} \sim E^{\alpha}$ where α had a value between 1.15 and 1.56 depending on the particle concentration. These values of α are in good agreement with the predicted value of $1 < \alpha < 2$ given in the conduction model for ER fluids [15].

Samples with a dispersive phase of higher viscosity (silicon oil with η_s= 350 mPa s) was also studied but rheological measurements were unstable making analysis difficult. The samples also showed lower ER effect than that of the presented samples. Hence, these high viscosity samples were not studied further. Samples with higher particle concentration were not prepared due to the high conductivity of the particles which would cause electric breakdown of the system at low electric fields.

4.2.3 Electrical properties of CC particles and CC particle dispersion

The dc conductivity of the as-produced CC particles was measured using a two electrode configuration. The measurement cell consisted of a cylindrical tube placed on a stainless steel support plate which served as one of the electrodes. A stainless steel piston with diameter equal to the inner diameter of the cylindrical tube was used as the second electrode ($A = 28.3$ cm^2). Carbon cone powder was poured into the cylinder, the cylindrical electrode was placed carefully on top and the height of the resulting powder column was manually measured. Measurements with varying column height and with various pressures were carried

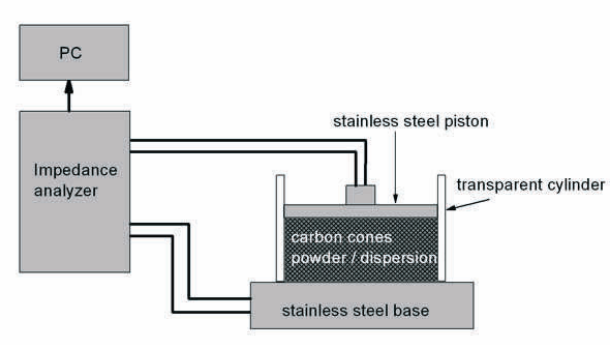

Figure 4.10: The experimental setup for impedance measurements.

out as the electrical properties are highly dependent on the packing of the powder. The ac conductivity of as-produced carbon cones powder was calculated to be Σ_p=0.2 S/m, at 50 Hz, 1 V rms and at a pressure of 0.87 kPa. This was determined using the relation $\Sigma_p = l/RA$, where l is the distance between the electrodes, A is the area of the electrode and R is the measured resistance of the powder.

Impedance measurements of a dispersion of 1.1 wt% CC in silicon oil was carried out using an impedance analyzer (Solartron SI 1260) together with an amplifier (Solartron 1294). The analysis was carried out using frequency sweep from $0.1 - 1 \cdot 10^6$ Hz, with the amplitude varying between 50-3000 mV. The impedance of the system was found to be strongly amplitude dependent. The dielectric constant of the dispersion of CC in silicon oil (1.1 wt%) was determined from the measured capacitance using the relation $\varepsilon_r = Cl/A$, where $\varepsilon_r = \varepsilon/\varepsilon_0$ is the relative dielectric constant and was determined to be $\varepsilon_r = 3.8$, evaluated at $1 \cdot 10^4$ Hz and 1 V rms. The dielectric loss factor was calculated from the conductance and is shown in figure 4.11. The local maxima at about 30 Hz represents the relaxation frequency of the system. According to literature [19, 53] a good ER effect is found for dispersions with relaxation frequencies in the range $100 - 1 \cdot 10^5$ Hz. Hence the low relaxation frequency observed for our system is in good agreement with the low ER effect observed. A small peak at $\sim$1 Hz which is difficult to observe in figure 4.11, is attributed to electrode polarization that is probably due to adsorbed water in the system. The 1 Hz peak increases with decreasing amplitude (not shown).

4.3 Viscosity measurements of a ferrofluid using magnetic holes

In the work presented in **P4** magnetic holes [54] have been used to predict the local viscosity of a ferrofluid (FF). A microrheological method which may be used for small sample volumes was developed. The experimental setup consisted of two pair of perpendicular coils producing

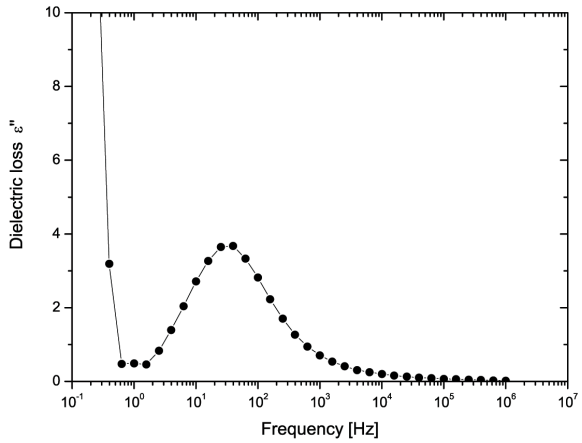

Figure 4.11: The dielectric loss factor for 1.1 wt% CC in silicon oil measured at 1 V rms. The relaxation frequency is found at the local maxima observed at approximately 30 Hz.

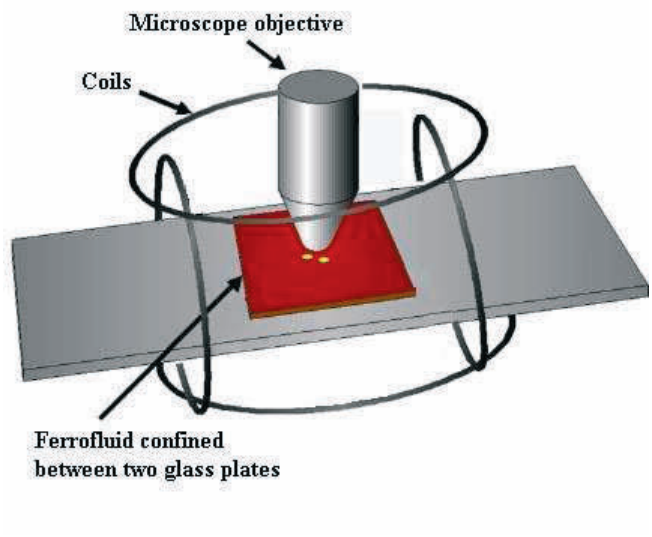

Figure 4.12: The setup of the magnetic hole cell with the magnetic coils for producing a rotating magnetic field.

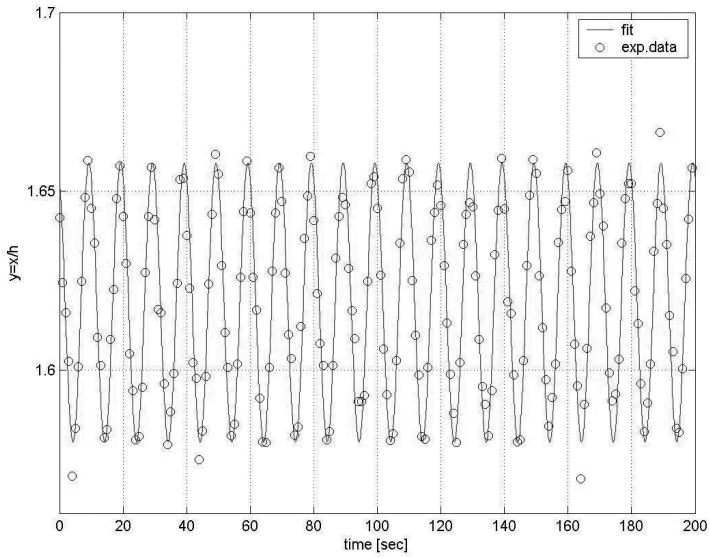

Figure 4.13: Separation distance vs time for the oscillating magnetic holes. The solid line is a sine curve fitted to the experimental data.

a rotating magnetic field in the x-z direction. The coil setup was placed on the sample stage of a microscope with a digital video camera, see figure 4.12.

A planer quasi 2D cell (Starna, type 20-C G 0.1 mm) with dimensions length: 38 mm, width: 8 mm and height 0.1 mm was used. Polystyrene spheres [55] with diameter 50 μm served as magnetic holes. The ferrofluid (EMG 901 and EMG 905 from Ferrotech [29]) with densities $\rho = 1.53$ and 1.24 g/cm^3 and susceptibilities $\chi_f = 3.0$ and 1.9, respectively were investigated. The ferrofluid and two magnetic holes were added to the cell. Then the cell was placed in the middle of the coils and the fields adjusted until a steady oscillation of the magnetic holes was achieved. The frequency of the oscillating field was low, 0.05 Hz in order to have laminar flow. The system was left to stabilize for at least one hour. After a stable oscillation was obtained, a video recording of the motion of the microspheres was carried out over a period of 10-20 minutes. The recorded video images were treated with an appropriate threshold level in order to get white particles on a black background. By using a Matlab program employing a particle tracking function the movement of the oscillating spheres where tracked and the relative distance between them computed. Finally a sine curve was fitted to the data as seen in figure 4.13. By taking into account friction forces from the walls of the cell containing the fluid and particles and the disturbance field produced by one particle on the other, the local fluid viscosity may be deduced, using theory briefly described in end of chapter 1.3.2. The details of this microrheological method are found in **P4**.

4.3.1 Carbon cone added ferrofluid

The addition of non-magnetic particles to ferrofluids is know to produce organized patterns (chains) in a magnetic field do to the alignment of the dipoles [56, 54]. Due to the unique nature of the CC particles we were interested in studying their behavior in a ferrofluid under the influence of a magnetic field. When adding CC particles to a ferrofluid we expected them to behave similar to magnetic holes and hence to see alignment which would result in increased magnetoviscosity. We also wanted to investigate the possibility of separation of particles within this system. However, there were many obstacles which limited the success of this study: Visual observation of the particles was impossible due to the opaque nature of the kerosene based ferrofluid which produced a low contrast between the fluid and particles. The use of waterbased ferrofluids could have been an option but this requires some surface treatment of the particles which could influence the nanoparticles of the FF. Also when carrying out magnetorheological measurements (as described in **P3**) with 1.5 wt% CC added ferrofluid, little or no increase in magnetoviscosity was found indicating no field alignment of the carbon particles. At low fields and low shear rates an increase was found but this was attributed to pure hydrodynamic effect of particle-particle interaction and the resistance to flow due to the bounded liquid layer around each particle. The low increase in magnetoviscosity might be due to slow particle orientation or because of particle aggregation. However, one would expect that the particles would dissolve well in the kerosene based liquid. The particles were used as received without any surface treatment. The investigation of a suitable surface treatment or coating of the CC particles that may increase the magnetoviscosity should be explored in the future.

4.4 Characterization of single particles

Various microscope techniques have been used during the work of this thesis, including optical microscopy, AFM (atomic force microscopy), STM (scanning tunneling microscopy) and SEM (scanning electron microscopy). As the author spent a great deal of time getting acquainted with and using the AFM/STM for characterization of single particles, a **technical report (TR)** included in the article section, has been written with the thought of serving as an aid for other people using the setup described. Hence AFM/STM is not further described in this section.

Optical microscope

For visual observations of structure formation of CC in silicon oil (**P2** and **P3**) and for the tracking of magnetic holes (**P4**) an optical microscope (Nikon Optiphot Biological Microscope) was used. The microscope has a standard video adapter where a digital camera (JVC 3CCD KY-F55 BE colour video camera with 768 x 576 pixels) was mounted. The camera has one CCD for each of the primary colors. The signal from the video camera goes to a monitor by the microscope and either a digital video recorder/player or a computer. Magnifications used varied between 40x and 400x.

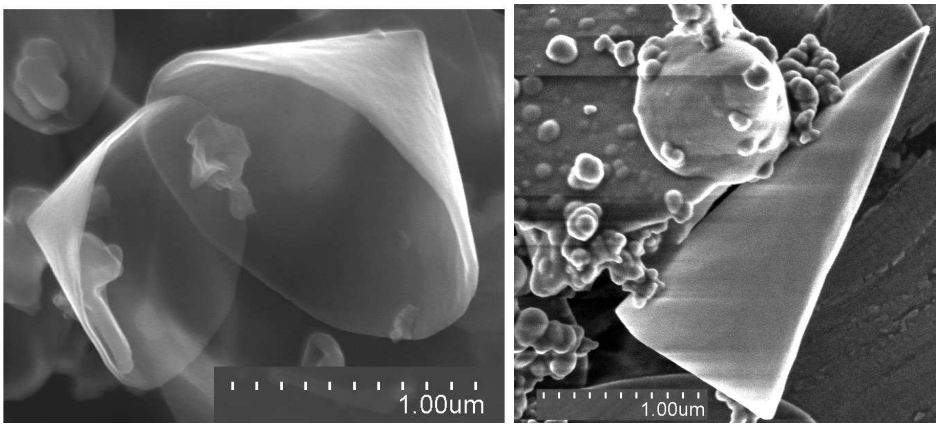

Figure 4.14: SEM images of carbon cones particles.

Scanning electron microscope

The SEM used during this thesis is an ultra-high resolution Hitachi S-4800. It has a Noran System Six energy dispersive spectrometer (EDS) for element analysis. The SEM has been used for characterization of CC particles and carbon nanotubes. Figure 4.14 show SEM images of carbon cones with variable apex angles. The samples were prepared by spreading dry CC powder on carbon tape or on aluminum foil. The intention was also to use the SEM to observe the orientation/organization of carbon cones particles after chain formation, but this was not achieved due to difficulties with removing residual oil without destroying the chains.

Chapter 5

Concluding remarks

In this thesis complex nanofluids of different kinds have been the subject of various investigations. The main focus was the use of carbon cone particles as the solid phase in both electrorheological fluids and magnetorheological fluids.

CC particles were dispersed in silicon oil and the electrorheological behavior studied. First the chain growth was studied proving that the CC particles form chains even at fields as low as 50 V/mm. The strength of the chains were investigated using electrorheological measurements. The dispersions show a weak ER effect as measured by the ER efficiency given by the relative increase in the viscosity under applied electric field. The relatively weak effect as compared to other ER fluids is contributed to the low relaxation frequency found to be 30 Hz and to the high conductivity of the particles. The chains formed under an electric field do not dissolve when the electric field is turned off. Hence dispersions of CC particles in silicon oil are not useful as ER fluids. However, the possibility of particle alignment by ac electric fields may be exploited for producing conductive composites with anisotropic conductivity.

The dispersion of CC particles in a ferrofluid showed little influence on the viscosity under an applied magnetic field. This could be due to poor particle dispersion. The dispersion of CC in ferrofluids must be further investigated and a method for surface coating of the particles should be explored. The behavior of the CC particles in ferrofluid under an applied magnetic field could be investigated using a water based ferrofluid and a suitable surface treatment of the particles in order to disperse them in such a system.

Finally the interaction of magnetic holes in a ferrofluid has been utilized to develop a microrheological method for measuring the local viscosity of the ferrofluid itself. By balancing the hydrodynamic and magnetic forces on two oscillating holes, the apparent viscosity may be extracted. The advantage of the method is the small sample volume needed, and that information about local rheological properties is obtained. A discrepancy between the calculated viscosity and the reference value was found, but this was attributed to the higher temperature of the ferrofluid. The temperature dependent viscosity must be further investigated in order to determine the accuracy of the method.

Bibliography

[1] D.J.Klingenberg. Magnetorheology:applications and challenges. *AIChE Journal*, 47(2):246–249, Februar 2001.

[2] H.J.Choi and M.S.Cho. Synthesis and electrorheology of mesoporous particle suspensions. *International Journal of Modern Physics B*, 16(17-18):2514–2520, 2002.

[3] I.M.Krieger and T.J.Dougherty. A mechanims for non-newtonian flow in suspensions of rigid spheres. *Trans. Soc.Rheol.*, 3(137-152), 1959.

[4] G.Y.Onoda and E.R.Liniger. Random loose packings of uniform spheres and the dilatancy onset. *Phys.Rev.Lett*, 64:2727, 1990.

[5] W.M.Winslow. Method and means for translating electrical impulses into mechanical force. US Patent 2,417,850, March 1947.

[6] W.M.Winslow. Induced fibration of suspensions. *Jour. Applied Physics*, 20:1137–1140, 1949.

[7] X.Pan and G.H.McKinley. Simultaneous measuremnt of viscoelesticity and electrical conductivity of en electrorheological fluid. *Langmuir*, 14:985–989, 1998.

[8] L.C.Davis. Polarization forces and conductivity effects in electrorheological fluids. *Journal of Applied physics*, 72(4):1334–1340, 1992.

[9] H.U.Mustafa, H.Usui, M.Ishizuki, I.Shige, and H.Suzuki. Rheological characteristics of non-spherical graphite suspensions. *Korea-Australia Rheology Journal*, 15(1):19–25, 2003.

[10] H.J.Choi, J.W.Kim, S.H.Yoon, R.Fujiura, M.Komatsu, and M.S.Jhon. Symthesis and electrorheolgical characterization of carbonaceous partilce suspensions. *Journal of Materials Science Letters*, 18:1445–1447, 1999.

[11] B.Powell. Preparation of electrorheological fluids using fullerenes and other crystals having fullerene-like anisotropic electrical properties. US Patent 5445759, 1995.

[12] T. Hao. Electrorheological fluids. *Advanced materials*, 13(24):1847–1857, 2001. review article.

[13] T.C.Halsey and W.Toor. Sturcture of electrorheological fluids. *Phys.Rev.Lett.*, 65(2):2820–2823, 1990.

[14] M.Parthasarathy and D.J.Klingenberg. Electrorheology;mechanisms and models. *Materials Science and Engineering*, R17:57–103, 1996.

[15] P.Atten, J.N.Foulc, and N.Flici. A conduction model of the elctrorheological effect. *J.Electrostatics*, 33:103–112, 1994.

[16] D.L.Klass and T.W.Martinek. Electroviscous fluids. 1.rheological properties. *Journal of Applied physics*, 38:67, 1967.

[17] W.Wen, X.Huang, and P.Sheng. Electrorheological fluids: structures and mechanisms. *Soft Matter*, 4:200–210, 2008.

[18] W.Wen, X.Huang, S.Yang, K.Lu, and P.Sheng. The giant electrorheological effect in suspensions of nanoparticles. *Nature Materials*, 2:727–730, 2003.

[19] F.Ikazaki, A.Kawai, K.Uchida, T.Kawakami, and K.Edamura. Mechanisms of electrorheology:the effect of the dielectric property. *J.Physics D:Applied physics*, 31:336–347, 1998.

[20] Y.Qi and W.Wen. Influence of geometry of particles on electrorheological fluids. *Journal of Physics D*, 35:2231–2235, 2002.

[21] A.Lengalova, V.Pavlinak, P.Saha, O.Quadrat, and J.Stejskal. The effect of dispersed particle size and shape on the electrorheological behaviour of suspencions. *Colloids and surfaces A*, 227:1–8, 2003.

[22] E.Svasand, G.Helgesen, and A.Skjeltorp. Chain formation in a complex fluid containing carbon cones and disks in silicon oil. *Colloids and surfaces A*, 308:67–70, 2007.

[23] M.K.Schwarz, W.Bauhofer, and K.Schulte. Alternating electric field induced agglometation of carbon black filled resins. *Polymer*, 43:3079–3082, 2002.

[24] J. Rabinow. The magnetic fluid clutch. *AIEE Trans*, 67:13081315, 1948.

[25] J.M.Ginder and L.C.Davis. Rheology of magnetorheological fluids, model and measurements. *Proc. of the 5th Inter. Conf. on ER Fluids, MR susp. and Ass. Techn.*, 1996.

[26] N.A.D'Souza and Z.Yang. Magnetorheology of multiwalled nanotube dispersion in mineral oil. *Jour. of Nano Research*, 1:40–49, 2008.

[27] W.H.Li, C.Lynam, J.Chen, B.Liu, X.Z.Zhang, and G.G.Wallace. Magnetorheology of single-walled nanotube dispersions. *Materials letters*, 61:3116–3118, 2007.

[28] S.Odenback. Magnetic fluids -suspensions of magnetic dipoles and their magnetic control. *Journal of physics; Cond.matter*, 15:S1497–S1508, 2003.

[29] Ferrotec Corporation, 40 Simon Street, Nashua, NH 03060-3075.

[30] E.Svasand, J.Akselvoll, G.Helgesen, and A.Skjeltorp. Local viscosity measurements using oscillating magnetic holes. *J.Appl.Phys*, 101:054910–054916, 2007.

[31] Michael Ströck. Allotropes of carbon. http://en.wikipedia.org/wiki/ Image:Eight_Allotropes_of_Carbon.png, Feb 2006.

[32] H.W.Kroto, J.R.Heath, S.C.O'Brien, R.F.Curl, and R.E.Smalley. C_{60}:buckminsterfullerene. *Nature*, 318(14):162–163, 1985.

[33] S. Iijima. Helical microtubules of graphitic carbon. *Nature*, 354(7):56–58, November 1991.

[34] K. Sattler and M. Ge. Observation of fullerene cones. *Chemical physics letters*, 220:192–196, 1994.

[35] S. Dimovski, J.A.Libera, and Y.Gogotsi. A novel class of carbon nanocones. *Material Research Society Symp.Proc.*, 706, 2002.

[36] J.Liu, W.Lin, X.Chen, S.Zhang, F.Li, and Y.Qian. Fabrication of hollow carbon cones. *Carbon*, 42:667–691, 2004.

[37] J.A.Jaszczak, G.W.Robinson, S.Dimovski, and Y.Gogotsi. Naturally occurring graphite cones. *Carbon*, 41:2085–2092, 2003.

[38] A.Krishnan. Graphitic cones and the nucleation of curved carbon surfaces. *Nature*, 388:451–454, July 1997.

[39] IFE. Hydrogen storage in carbon material. Norwegian patent No. 307986 (2000), US patent No. 6,290,753 (2001), EPO Patent No. 1051530 (2004).

[40] Kvaerner ASA. For production of micro domain particles by use of a plasma process. patent No. PCT/NO98/00093.

[41] n tech. http://www.n-tec.no.

[42] X. Fan, R. Buczko, A. A. Puretzky, D. B. Geohegan, J. Y. Howe, S. T. Pantelides, and S. J. Pennycook. Nucleation of single-walled carbon nanotubes. *Phys. Rev. Lett.*, 90(14):145501, Apr 2003.

[43] T.Wakabayashi and Y.Achiba. A model for the c_{60} and c_{70} growth mechanism. *Chem. Phys. Lett.*, 190:465–468, 1992.

[44] M.M.J.Treacy and J.Kilian. Designability of graphitic cones. *Mat.Res. Soc.Proc.*, 675, 2001.

[45] T.A.Adams. Properties of carbon nanotubes. http://www.pa.msu.edu /cmp/csc/nanotube.html.

[46] M.A.J.Veld. The wondrous world of carbon nanotubes. Technical report, Eindhoven University of Technology, 2003.

[47] P.G.Collins Philip and P.Avouris. Nanotubes for electronics. *Scientific American*, pages 62–69, dec 2000.

[48] E.G.Rakov. Methods for preparation of carbon nanotubes. *Russian Chemical Reviews*, 69(1):35–52, 2000.

[49] T.Lutz and K.J.Donovan. Macroscopic scale separation of metallic and semiconducting nanotubes by dielectrophoresis. *Carbon*, 43(12):2508–2513, 2005.

[50] H.Heiberg-Andersen, A.T.Skjeltorp, and K.Sattler. Carbon nanocones: A variety of non-crystalline graphite. International Workshop of Non-Crystalline Solids (IWNCS), Portugal, 2008, in press.

[51] A.C. Lau. Electrokinetic properties of carbon black and graphitized carbon black. *Colloids and surfaces*, 18:93–104, 1986.

[52] Y.Lan, X.Xu, S.Men, and K.Lu. The conductivity dependence of the shear stress in electrorheological fluids. *Applied physics letters*, 73(20):2908–2910, 1998.

[53] H.Block and J.P.Kelly. Electro-rheology. *J.Phys.D:Appl.Phys*, 21:1661–1677, 1988.

[54] A.T. Skjeltorp. One- and two-dimensional crystallization of magnetic holes. *Phys. Rev. Lett.*, 51:2306, 1983.

[55] J. Ugelstad, P.C. Mørk, K.H. Kaggerud, T. Ellingsen, and A. Berge. Swelling of oligomer-polymer particles - new methods of preparation of emulsions and polymer dispersions. *Adv. Colloid. Int. Sci.*, 13:101, 1980.

[56] S.Hess, J.B.Hayter, and R.Pynn. A comparison of molecular dynamics and analytic calculation of correlation in an aligned ferrofluid. *Molecular Physics*, 53(6):1527–1533, 1984.

[57] P. Umek. An effective surfactant-free isolation procedure for single-wll carbon nanotubes. *Carbon*, 40:2581–2585, 2002.

[58] J. Chen, R.C. Haddon, and M.A. Hamon. Method of solubilizing unshortened carbon nanotubes in organic solutions. Patent, US 6,368,569, B1.

[59] W.Huang. Sonication-assisted functionalization and solubilization of carbon nanotubes. *Nano Letters*, 2(3):231–234, 2002.

[60] Y.Qin. " large-scale preparation of solubilized carbon nanotubes. *Chem. Mater*, 15:3256–3260, 2003.

[61] M.F.Islam. High weight fraction surfactant solubilization of single-wall carbon nanotubes in water. *Nano Letters*, 3(2):269–273, 2003.

[62] R.Bandyopadhyaya. Stabilization of individual carbon nanotubes in aqueous solutions. *Nano Letters*, 2(1):25–28, 2002.

Appendix A

Dispersion of carbon materials

A.1 Introduction

The dispersion of carbon cones and carbon nanotubes is important for further use of these materials in i.e composites, for deposition on electronic chips and in general in order to study single particle properties. Many methods concerning solubilization of CNT have been reported [57, 58, 59, 60], many of which require complex chemical treatment. However, some simpler methods have also been reported [61, 62]. The latter methods involve surfactants to help over win the strong attractive forces between the particles and using ultra sonication treatment. The methods used for CNTs were also employed for the dispersion of carbon cones. In all cases the degree of dispersion rather than the stability of the dispersion was the main concern. This was due to the fact that the dispersions were used only as a starting point of sample preparation for AFM/STM characterization (for details see **TR**). In the case of the study of electrorheological fluids the solutions were stable within the time frame of the experiments.

A.2 Dispersing carbon cones

Carbon cones powder (CC), was provided by Carbon Cones AS. Distilled water, isopropanol and silicon oil (Dow Corning, 200/100cS Fluid) were employed as dispersants for dispersing the carbon material.

For the preparation of electrorheological fluids, silicon oil was used as the dispersing media. For visual observation of chain formation dilute samples with concentrations of around 0,1 wt % were used. For electrorheological measurements the dispersions had concentrations of 2-20 vol%. After ultra sonication of 20 min the dispersions appear homogeneous and remained stable for some days before sedimentation was observed. The degree of dispersion was confirmed using optical microscopy. The stability of the dispersions was determined by visual observation. The time evolution of the sedimentation is shown in figure A.1.

For AFM characterization samples were prepared from solutions of CC in isopropanol. The dispersions were dilute since the main purpose of the dispersion was to prepare samples

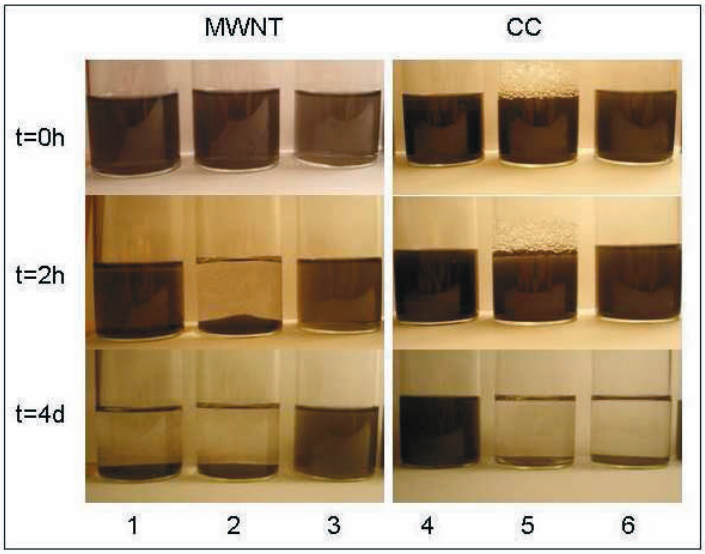

Figure A.1: Dispersion stability; comparison between MWNT and carbon cones dispersed in various liquids. Samples 1, 2(with surfactant) and 6 were prepared with isopropanol, 3 and 4 with silicon oil and 5 with water and surfactant.

for AFM characterization with the goal of imaging singular cones. After sonication a drop of the dispersion was placed on a heated mica substrate. This ensured rapid evaporation of the fluid, decreasing particle aggregation. The dispersion showed low stability. Sedimentation occurred within 2-24 hours depending on the concentration.

To disperse carbon cones in water, a successful recipe [61] of dispersion of carbon nanotubes in water, using NaDDBS was applied. Sedimentation took place within hours. Comparably the nanotube dispersion remained stable for more than a year. This is probably due to the larger size of the carbon cones/disk particles which are not subjected to large Brownian motion and therefor settle more easily.

Other dispersants like ethanol and toluene also disperse carbon cones particles well. The stability is similar to that of isopropanol.

A.3 Dispersing multiwalled carbon nanotubes

As produced MWNTs (provided by n-tech) were mixed with different dispersants and surfactants and treated with ultrasound. The stability and dispersing abilities of the different dispersive phases were studied over time. The dispersive phases used were distilled water and isopropanol and silicon oil.

As carbon is highly hydrophobic, water alone cannot solubilize carbon material. However with the aid of a surfactant it is possible. In this study we used the surfactant NaDDBS (Sodium dodecylbenzenesulfonate). The MWNTs were mixed with the surfactant and deionized water and thereafter treated by sonication for 2 hours. The dispersing effect was confirmed by optical microscopy, showing little or no aggregates. The stability of some of the solutions are shown in figure A.1. The solutions proved to be stable even after one year.

MWNT were also solubilized in isopropanol with and without surfactant (NaDDBS). MWNT dispersed in isopropanol formed a homogeneous solution after ultra sonication, but the solution was not stable for a long period of time. Typically less than 12 hours. An advantage of using isopropanol as a dispersant was that there was no "ring-effect" when placing a drop of the solution on a mica substrate for AFM characterization. The MWNT still suffered aggregation, but the samples showed smaller agglomerations and the aggregates were more evenly distributed over all the mica, compared to samples prepared with water and surfactant. This is due to the lower surface tension of isopropanol compared to that of water.

The dispersing effect was again confirmed by optical microscopy. No aggregates were observed. It was observed that NaDDBS does not dissolve well in isopropanol, and miscelles of NaDDBS with small amounts of carbon material were observed.

MWNT was easily dispersed in silicon oil (Dow Corning, 200/100cS Fluid) by ultra sonication and was stable for at least 4 days.

A.4 Conclusion

General observations are that CC and MWNT may be easily dispersed in isopropanol and silicon oil. In water surfactant is needed. In general CC dispersions are stable for a longer time than MWNT, except for MWNT in water with NaDDBS which was stable for more than a year. For AFM sample preparation particles dispersed in isopropanol is convenient while for electrorheology silicon oil is a good choice due to its low conductivity.

Appendix B

Data analysis for oscillating magnetic holes

A general overview over Matlab programs and functions used to analyze magnetic hole data are found in the manuals "Magnetic hole analysis procedure" and "Magnetic hole programs" found in the Light laboratory. In this section I will give some extra information for future users of the programs concerning special parameters/functions that need extra attention.

"*magnetic_hole.m*" is the main file and includes many other subfunctions. These functions must be run the first time and also some parameters in some of the functions must be set;

"*Mag_hole_pos.m*" finds the position of the spheres using the function *pkfn.m* which locates bright peaks above set threshold. For *pkfn.m* to work the image files are first treated with a band pass function *B=bpass(A,1,13)* where the last nr is approximately the diameter in pixels which must be an odd number. In the function *pkfn.m* the threshold level must be set and depends on the experimental conditions (size of spheres, brightness etc). The diameter (in pixels) of the spheres must also be set. The program then uses the function *cntrd.m* to locate the center of the bright spots. The parameter which must be set for this function is the diameter which must be an odd number. Finally the program uses the function *track.m* to get the position of the spheres from each image. Here the maximum displacement between two frames must be set for the continuous tracking to be valid. Default is 10 pixels. The time vector in the program is written for images of 1 frame pr second.